Knockout of liver fluke granulin, *Ov-grn-1*, impedes malignant transformation during chronic infection with *Opisthorchis viverrini*

Short title: Knockout of liver fluke growth factor impedes bile duct cancer

Sujittra Chaiyadet[1, 2, 3] Sirikachorn Tangkawattana[3,4], Michael J. Smout[3,5,], Wannaporn Ittiprasert[3,6], Victoria H. Mann[6], Raksawan Deenonpoe[7], Patpicha Arunsan[1,6], Alex Loukas[5,8], Paul J. Brindley[6, 8], Thewarach Laha[1,8]

[1] Department of Parasitology, Faculty of Medicine, Khon Kaen University, Khon Kaen, 40002 Thailand

[2] Tropical Medicine Graduate Program, Academic Affairs, Faculty of Medicine, Khon Kaen University, Khon Kaen, 40002 Thailand

[3]equal contribution

[4] Faculty of Veterinary Medicine, Khon Kaen University, Khon Kaen, Thailand, and WHO Collaborating Center for Research and Control of Opisthorchiasis, Tropical Disease Research Center, Khon Kaen University, Khon Kaen 40002, Thailand

[5] Centre for Molecular Therapeutics, Australian Institute of Tropical Health and Medicine, James Cook University, Cairns, Queensland, 4878, Australia

[6] Department of Microbiology, Immunology and Tropical Medicine, and Research Center for Neglected Diseases of Poverty, School of Medicine & Health Sciences, George Washington University, Washington, D.C. 20037, USA

[7]Department of Pathology, Faculty of Medicine, Khon Kaen University, Khon Kaen, 40002 Thailand

[8]Correspondence: Thewarach Laha, email, thewa_la@kku.ac.th; Alex Loukas, email, alex.loukas@jcu.edu.au; Paul Brindley, email, pbrindley@gwu.edu, Twitter, @PaulJBrindley

Abstract

Infection with the food-borne liver fluke *Opisthorchis viverrini* is the principal risk factor for cholangiocarcinoma (CCA) in the Mekong Basin countries of Thailand, Lao PDR, Vietnam, Myanmar and Cambodia. Using a novel model of CCA, involving infection with gene-edited liver flukes in the hamster during concurrent exposure to dietary nitrosamine, we explored the role of the fluke granulin-like growth factor *Ov*-GRN-1 in malignancy. We derived RNA-guided gene knockout flukes (*ΔOv-grn-1)* using CRISPR/Cas9/gRNA materials delivered by electroporation. Genome sequencing confirmed programmed Cas9-catalyzed mutations of the targeted genes, which was accompanied by rapid depletion of transcripts and the proteins they encode. Gene-edited parasites colonized the biliary tract of hamsters and developed into adult flukes, however less hepatobiliary tract disease manifested during chronic infection with *ΔOv-grn-1* worms in comparison to hamsters infected with control gene-edited and non-edited parasites. Specifically, immuno- and colorimetric-histochemical analysis of livers revealed markedly less periductal fibrosis surrounding the flukes and less fibrosis globally within the hepatobiliary tract during infection with *ΔOv-grn-1* genotype worms, minimal biliary epithelial cell proliferation, and significantly fewer mutations of *TP53* in biliary epithelial cells. Moreover, fewer hamsters developed high-grade CCA compared to controls. The clinically relevant, pathophysiological phenotype of the hepatobiliary tract confirmed a role for this secreted growth factor in malignancy and morbidity during opisthorchiasis.

Keywords

Infection-associated cancer; liver fluke; opisthorchiasis; cholangiocarcinoma; CRISPR/Cas; knockout; granulin

Author summary

Infection with the human liver flukes, *Opisthorchis viverrini*, *O. felineus* and *Clonorchis sinensis* remains a public health concern in regions where these parasites are endemic. *O. viverrini* is endemic in the Mekong River drainage countries of including Thailand and the Lao People's Democratic Republic. Infection follows the consumption of undercooked freshwater fish harboring the parasite. Liver fluke infection, opisthorchiasis, is associated with diseases of the liver and bile ducts including cancer of the biliary tract, cholangiocarcinoma, a cancer with a poor prognosis. This report characterizes for the first time experimental infection with gene-edited *O. viverrini* liver flukes during concurrent exposure to nitrosamine in a rodent model of liver fluke infection-associated cancer. Cancer development was slowed in hamsters infected with the parasite following CRISPR-based knock-out mutation and loss of a parasite gene known to stimulate growth of cells lining the bile ducts. These findings describe a new model for investigation of risk factors for infection-associated cholangiocarcinoma and to assess efficacy of anti-infection/anti-cancer vaccines.

83 **Introduction**

84 Liver fluke infection caused by species of *Opisthorchis* and *Clonorchis* remains a major public
85 health problem in East Asia and Eastern Europe. Infection with *Opisthorchis viverrini* is endemic
86 in Thailand and Laos, where ~10 million people are infected with the parasite. Opisthorchiasis is
87 associated with hepatobiliary diseases including cholangiocarcinoma (CCA), bile duct cancer (1,
88 2). Northeast Thailand reports the world's highest incidence of CCA, > 80 per 100,000 in some
89 provinces. Indeed, the International Agency for Research on Cancer of the World Health
90 Organization classifies infection with *O. viverrini* as a Group 1 carcinogen, i.e. definitely
91 carcinogenic in humans (1, 3, 4).
92

93 Which features or consequences of parasitism by the liver fluke definitely initiate malignant
94 transformation to CCA have yet to be ascertained notwithstanding that opisthorchiasis is the
95 principal risk factor for CCA in regions where this neglected tropical disease remains endemic
96 (1, 4-6). Some factors can be expected to more important than others and the impact of these
97 factors should be quantifiable. Different worm burdens play a role, based on rodent models of
98 liver fluke infection associated CCA (7), as does concurrent exposure to nitrosamines in
99 fermented foods (8, 9) that are culturally important dietary staples in countries of the Lower
100 Mekong River basin (5). Moreover, dose-dependent, synergistic effects of the liver fluke and
101 nitroso-compounds have been documented (7, 10). To survive within the host, parasitic
102 helminths actively release excretory/secretory (ES) proteins and other mediators with diverse
103 effects and roles at the host-parasite interface (11, 12). This interaction is considered to
104 manipulate host cellular homeostasis and, moreover, to underpin malignant transformation
105 during chronic opisthorchiasis, but the molecular mechanisms by which these processes remain

106 inadequately understood (13). Focusing on the contribution of liver fluke ES to carcinogenesis,
107 we targeted the *O. viverrini* granulin-like growth factor, *Ov*-GRN-1, a prominent component of
108 the ES complement that we had determined previously induces phenotypic hallmarks of cancer
109 (14, 15). *Ov*-GRN-1 and other ES components including extracellular vesicles enter
110 cholangiocytes, the epithelial cells that line the biliary tract, and drive cellular signaling that
111 promotes carcinogenesis, including cellular proliferation and migration, angiogenesis and wound
112 healing (16). We have confirmed the role of *Ov*-GRN-1 in driving proliferation of bile duct
113 epithelial cells (cholangiocytes) by genetic manipulation of its expression in the liver fluke both
114 by RNA interference and RNA-guided gene knockout (15, 17, 18). Moreover, we have shown
115 that infection of hamsters with the gene edited, infectious stage of the live fluke was feasible and
116 that proliferation of biliary epithelia is markedly suppressed during infection with the *ΔOv-grn-1*
117 (*Ov-grn-1-/-*) flukes (18).

118

119 There is an established and instructive model of the pathogenesis of CCA in experimentally
120 infected hamsters, *Mesocricetus auratus* that is thought to replicate the epidemiology and
121 pathogenesis of chronic human opisthorchiasis (1). In this model, malignancy manifests within a
122 few months following infection with metacercariae of the parasite and concurrent exposure to
123 otherwise sub-carcinogenic levels of dietary nitrosamine (7, 19, 20). In the hamster, chronic
124 opisthorchiasis provokes periductal fibrosis, which, coincident with exposure to the nitric oxide
125 carcinogen facilitates cholangiocyte proliferation, epithelial hyperplasia, DNA damage, and
126 allied biliary tract lesions (21), which can culminate in CCA (22). Using this model, here we
127 investigated the outcome of infection of hamsters with gene-edited *O. viverrini* liver flukes in
128 relation to fluke-induced periductal fibrosis and malignant transformation. For this investigation,

129 hamsters were infected with juvenile flukes that had been genetically modified using CRISPR
130 before infection. Specifically, following up on our earlier study (18) which focused on knockout
131 of the *Ov-grn-1* gene, here we included as comparators juvenile flukes gene-edited for a second
132 virulence factor, tetraspanin (*Ov-tsp-2*) (23), which also networks at the host-parasite interface
133 (24, 25) and, as controls, flukes subjected to CRISPR transfection by an irrelevant (non-
134 targeting) guide RNA (26).
135
136 Immuno- and colorimetric-histochemical analysis of thin sections of liver revealed markedly less
137 fibrosis during infection with *ΔOv-grn-1* worms, reduced proliferation of cholangiocytes,
138 substantially less expression of mutant forms of the p53 tumor suppressor protein and, overall,
139 diminished malignancy of the liver. The clinically relevant, pathophysiological phenotype
140 confirmed a role for *Ov*-GRN-1 in morbidity and malignancy during opisthorchiasis. Moreover,
141 these findings underscored the utility and tractability of CRISPR-based genome editing for
142 addressing gene function, essentiality, and pathogenesis in parasitic helminths generally.
143
144 **Results**
145
146 **Hamster model of malignant transformation during infection with gene-edited**
147 ***Opisthorchis viverrini***
148 To investigate the effect of programmed gene knockout (KO) in *O. viverrini*, two experiments
149 were undertaken in which hamsters were infected with newly excysted juveniles (NEJs) of *O.*
150 *viverrini* that had been subjected to programmed KO . The CRISPR/Cas systems were delivered
151 by electroporation of plasmids encoding guide RNAs specific for *Ov-grn-1*, *Ov-tsp-2* and an

152 irrelevant (control) guide RNA. All groups received plasmids encoding the Cas9 nuclease from
153 *Streptococcus pyogenes*. Figure 1A illustrates the experimental approach and timelines, the
154 findings from which we present below. Initially, juvenile flukes were subjected to transfection
155 after which reduction in transcription of the targeted genes, *Ov-grn-1* and *Ov-tsp-2*, was verified.
156 Subsequently, following successful KO of transcription *in vitro*, additional juvenile *O. viverrini*
157 were transfected before infection of hamsters. The goal of Experiment 1 was to assess impact of
158 KO on the worm burden. At necropsy14 weeks after infection, the entire liver was examined,
159 the worms were recovered and counted, and transcriptional changes were investigated in the
160 worms. With Experiment 2, the primary goal was establishment and assessment of disease
161 burden including malignant transformation during infection. Given that livers from the hamsters
162 in Experiment 2 were fixed at necropsy, worm burdens could not be established directly because
163 recovery of the flukes is a process that damaged the liver and biliary tract and, accordingly, was
164 incompatible with histological examination of infection-associated disease. Consequently, only a
165 small number flukes were available from Experiment 2 and these that were available were
166 collected incidentally during preparation of the liver lobes for fixation. Nonetheless, this sample
167 of the flukes from each of the three groups was sufficient to assess the performance and level of
168 programmed KO although total worm burden was unavailable. Nonetheless, the findings from
169 Experiment 2 provided the first description of gene-edited flukes in chronically-infected
170 hamsters, i.e., with duration of infection beyond eight weeks and, additionally, the first time

programmed mutation of the liver fluke genome has been combined with exposure to dietary nitrosamine in the hamster-liver fluke model of human CCA.

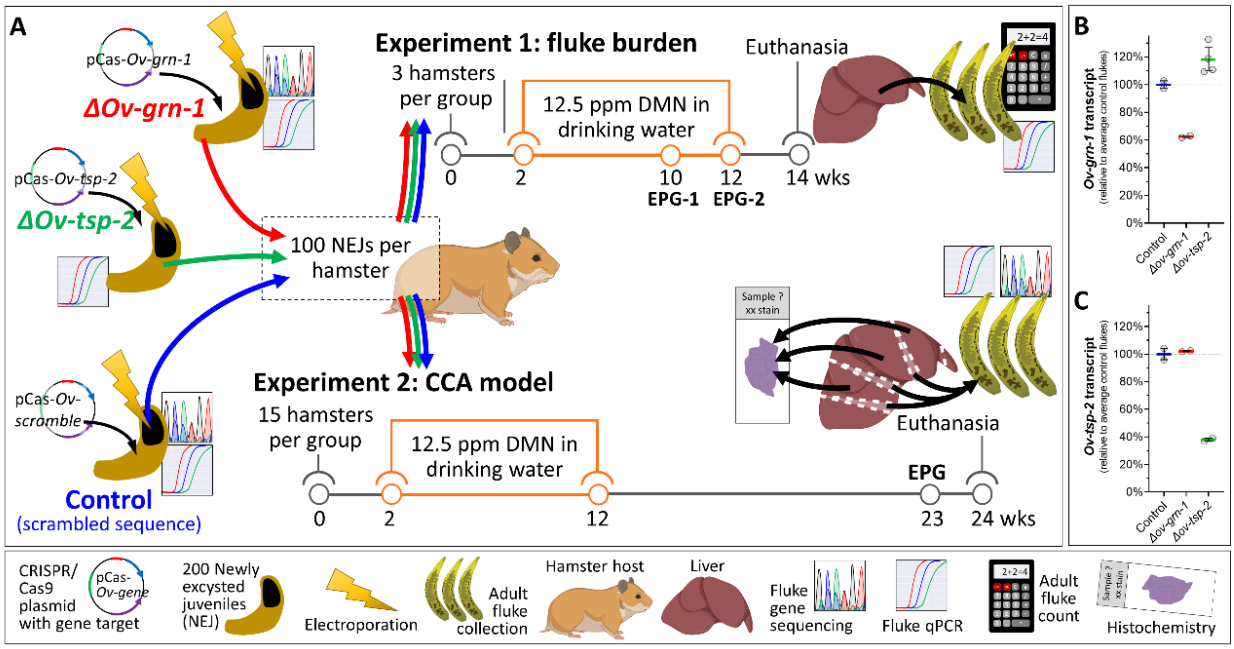

Figure 1. Schematic overview of the experimental design. *Hamsters were infected with juvenile Opisthorchis viverrini worms that had been subjected to gene knockout. Two experiments were conducted. (**A**). The goal of experiment 1 was to assess the impact of CRISPR/Cas9 editing on fluke survival. The goal of experiment 2 was to assess the influence of gene knockout on pathogenesis and malignant transformation. Groups of hamsters were infected with flukes transfected with CRISPR/Cas9 plasmids targeting either Ov-grn-1 (red, ΔOv-grn-1), Ov-tsp-2 (green, ΔOv-tsp-2), or irrelevant guide RNA (blue, control) and exposed to dimethyl nitrosamine (DMN) in the drinking water. At timepoints indicated for each experiment, fecal egg numbers were measured as eggs per gram of feces (EPG). Experiment 1: From the livers of euthanized hamsters, all the flukes were recovered and transcript levels assessed. Experiment 2: Liver lobes were sectioned and stained for histochemical analysis. Flukes incidentally released from bile ducts were collected and assessed for gene knockout. Before infection, transcript levels of Ov-grn-1 (**B**) and Ov-tsp-2 (**C**) were assessed in juvenile flukes. Transcript levels established by qPCR were plotted relative to average control transcript levels from 2-4 biological replicates; average shown with colored bar and with 95% confidence interval error bars. Population statistics were generated from resampling 1000 times with replacement bootstrap analysis of untransformed delta-delta Ct values (derived from Figure S1). (Elements of the figure were created with BioRender.com with copyright and licensing permission.)*

Changes in transcription of the targeted genes induced by programmed mutations were monitored by RT-qPCR in newly excysted juveniles (NEJs) (Figure S1). Control (irrelevant

197 gRNA) group flukes was used to normalize expression level from 100% (no change) to 0%
198 (complete ablation of expression) (Figure 1B, C). For the *ΔOv-grn-1* group, *Ov-tsp-2* was used
199 as an off-target gene control, and *Ov-grn-1* was used as an off-target control for the *ΔOv-tsp-2*
200 group. Relative to the control group, *Ov-grn-1* transcript levels were substantially reduced in the
201 *ΔOv-grn-1* flukes (bootstrapped average, 95% confidence interval [CI]: 62.4%, 61.8-63.1%)
202 whereas the transcription of *Ov-tsp-2* increased marginally (< 20% change) in the *ΔOv-grn-1*
203 flukes (117.8%, 95% CI: 110.2-127.0%) (Figure 1B). Transcription of *Ov-tsp-2* was substantially
204 reduced in the *ΔOv-tsp-2* flukes (37.9%, 95% CI: 36.7-39.1%). Levels of *Ov-grn-1* transcripts
205 (102.1%, 95% CI: 101.8-102.5%) were unchanged (Figure 1C). This outcome revealed gene-
206 specific, on-target knockout at the *Ov-grn-1* and *Ov-tsp-2* loci. Gene expression analyses were
207 restricted to the two targeted genes and hence we cannot conclude that off-target mutations did
208 not occur.
209
210 **Differential outcomes for adult flukes following knockout of *Ov-grn-1* and *Ov-tsp-2***
211 In Experiment 1, feces were sampled at both weeks 10 and 12 after infection (Figure 1A).
212 Significant differences in fecal egg counts (EPG) were not apparent among the three groups
213 (Figure 2A). Hamsters were euthanized and necropsied at week 14 to investigate the numbers of
214 adult *O. viverrini*. There were 60.0±3.46 (mean ± SEM), 36.7±3.48, and 21.3±2.96 worms in the
215 control, *ΔOv-grn-1*, and *ΔOv-tsp*-2 groups, respectively, reflecting reductions of 38.9% for *Ov-*
216 *grn-1* and 64.5% for *Ov-tsp*-2 (Figure 2B). A trend was apparent toward increased egg burdens
217 in hamsters with higher worm burdens but the correlation not statistically significant (Figure S2).
218

219 Of the worms recovered in Experiment 1, gene transcript levels relative to the control flukes
220 were assessed for 10-13 flukes from each of the three hamsters in each group. Transcript levels
221 (Figure S3) of both genes expressed by the control parasites clustered around 100% of wild-type
222 fluke expression levels with bootstrap averages of 114.1% (95% CI: 104.2-126.5%) and 103.2%
223 (95% CI: 98.4-107.5%) (Figure 2C, D). Transcript levels for *Ov-grn-1* ranged broadly in the
224 *ΔOv-grn-1* flukes from no change (~100%) to complete ablation (~0%) and, overall, were
225 substantially reduced at 11.8% (95% CI: 4.5-28.8%) of levels seen in wild-type flukes (Figure
226 2C). This phenotypic range, no change to ablation of transcripts in *Ov-grn-1,* was similar to our
227 previous findings . In contrast to the juvenile flukes, where there was substantial knockdown of
228 *Ov-tsp*-2 (Figure 1C), transcript levels were not markedly reduced in adult *ΔOv-tsp*-2 flukes
229 (82.5%, 95% CI: 73.6-91.5%) compared to the controls (103.2%, 95% CI: 98.4-103.2%) (Figure
230 2D). Indeed, most flukes in the *ΔOv-tsp*-2 group were unchanged with only two individual
231 flukes exhibiting > 50% reduction in *Ov-tsp*-2 expression. We posit that this marked difference,
232 in comparison to transcript levels for *Ov-tsp*-2 in juvenile flukes, i.e. reduced by 62.1%, in
233 addition to the 65% reduction of worms recovered at necropsy, *Ov-tsp-2* KO led to a lethal
234 phenotype and that flukes of this genotype failed to survive *in vivo*. This contrasted with *Ov-grn-*
235 *1* KO where the majority of flukes of the *ΔOv-grn-1* genotype survived even though transcription
236 of *Ov-grn-1* was not detected in four of 36 flukes, and 10 of 36 exhibited *Ov-grn-1* transcript
237 levels < 5% of levels expressed by the control worms.

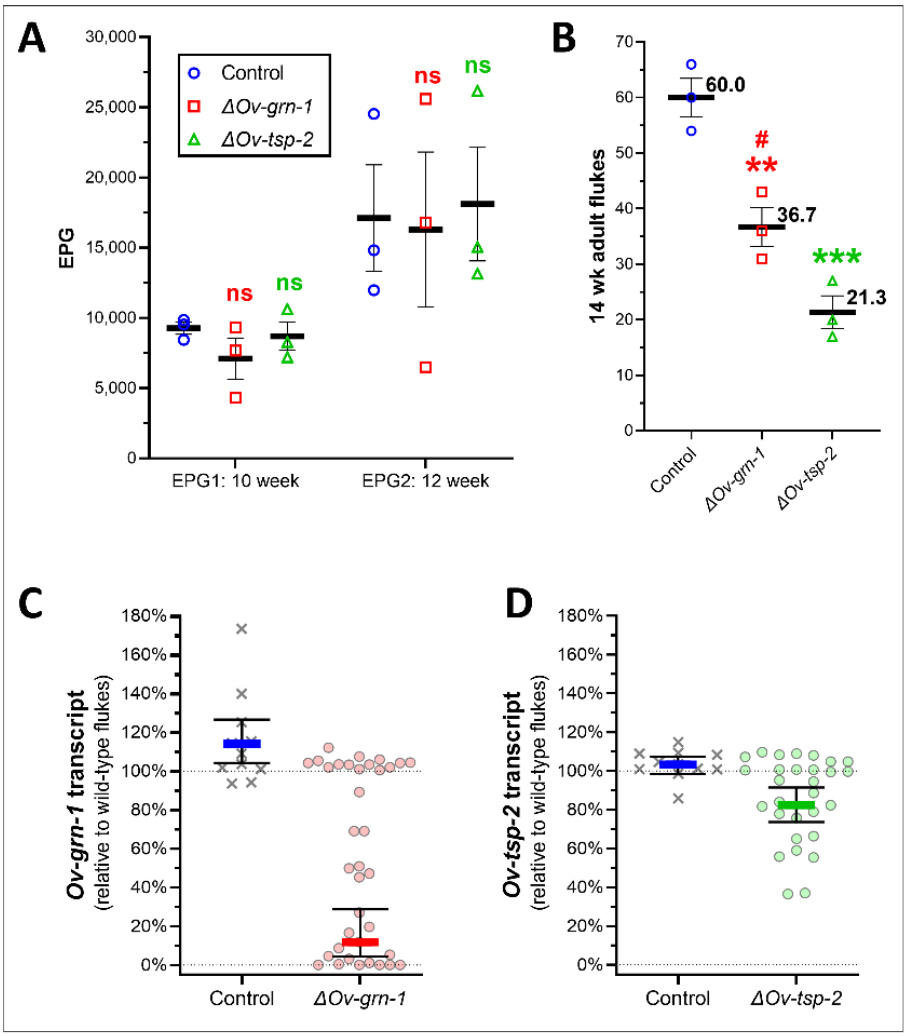

Figure 2. Liver fluke burden and levels of gene transcription. *Fecundity, worm numbers, and gene expression levels were determined at 10-14 weeks (Experiment 1) after infection of the hamsters with 100 gene edited juveniles, and from three hamsters per group. Number of eggs per gram of feces (EPG) from each hamster at weeks 10 and 12* ***(A)*** *and worm numbers at week 14* ***(B)*** *showing mean (horizonal black line) and SEM bars. Each treatment group was compared to control group with 2-way ANOVA with Holm-Sidak multiple comparison: ns = not significant; **, P ≤ 0.01; ***, P ≤ 0.001, and ΔOv-grn-1 against ΔOv-tsp-2: #, P ≤ 0.05. Gene transcript levels of Ov-grn-1* ***(C)*** *and Ov-tsp-2* ***(D)*** *were determined by qPCR for 10 to 13 flukes from each animal (30-39 total per group) and plotted with each data point representing the transcript level of an individual fluke relative to wild-type flukes. Resample with replacement bootstrap analysis (B=1000) of ddCT scores (Figure S3) used to generate population average, as denoted by the thick colored line and 95% confidence interval error bars.*

257 **Parasitological impact of gene knockout**
258
259 Quantitative assessment by histopathological and histochemical analysis of hepatobiliary disease
260 at 24 weeks of infection was a primary goal for Experiment 2. Accordingly, determining the
261 number of surviving liver flukes was not feasible because the liver and its intrahepatic biliary
262 tract, occupied by the parasites, was necessarily fixed in formalin at necropsy for downstream
263 histological processing and analysis. Nonetheless, we collected a sample of the resident *O.*
264 *viverrini* flukes before formalin fixation of the liver for molecular screening to assess the
265 efficacy of programmed gene knockout. As an accepted correlate of the number of worms
266 parasitizing each hamster (27), fecal egg counts (as eggs per gram of feces, EPG) were
267 determined at the time of necropsy. EPG values ranged broadly among the groups (Figure 3A),
268 with feces of the control fluke infected hamsters displaying the highest EPG values, median of
269 11,062 EPG (95% CI: 4,814-26,536), the *ΔOv-grn-1* group, 5,267 EPG (95% CI: 2,695-8535),
270 and the *ΔOv-tsp-2 group,* 4,530 EPG (95% CI: 518-10,227) in the same rank order in numbers of
271 worms recovered from these groups in Experiment 1 (Figure 2B). All the groups showed
272 substantial variation; the average EPG of *ΔOv-grn-1* hamsters was not significantly different to
273 controls whereas the *ΔOv-tsp-2* group had a significantly lower median EPG than the control
274 group ($P \leq 0.05$).
275
276 Adult worms recovered from Experiment 2 hamster livers examined at 24 weeks after infection
277 were evaluated for targeted gene transcripts by qPCR. *Ov-grn-1* transcript levels (Figure S4) of
278 adult *O. viverrini* from *ΔOv-grn-1* infected hamsters were substantially decreased down to a
279 bootstrapped average of 10.6% relative to wild-type flukes (95% CI: 3.1-30.9%) compared to the
280 control group with 91.0% (95% CI: 84.1-97.5%) (Figure 3B). In contrast, numbers of flukes in

281 the *ΔOv-tsp-2* treatment group were similar, at 101.1% (95% CI: 91.1-111.3%) of wild-type
282 flukes 98.5% (95% CI: 82.3-114.6%) of the controls (Figure 3C). With Experiments 1 and 2
283 showing the surviving *ΔOv-tsp-2* group worms expressing *Ov-tsp-2* at levels comparable to the
284 control flukes, we posit that substantial *Ov-tsp-2* gene edits were lethal, and worms that survived
285 to maturity likely had not undergone gene editing and/or few of the cells in the worms had been
286 edited. Although we retained the *ΔOv-tsp-2* group for comparison of pathogenesis, the genotype
287 of the flukes from this group was not investigated further.

288

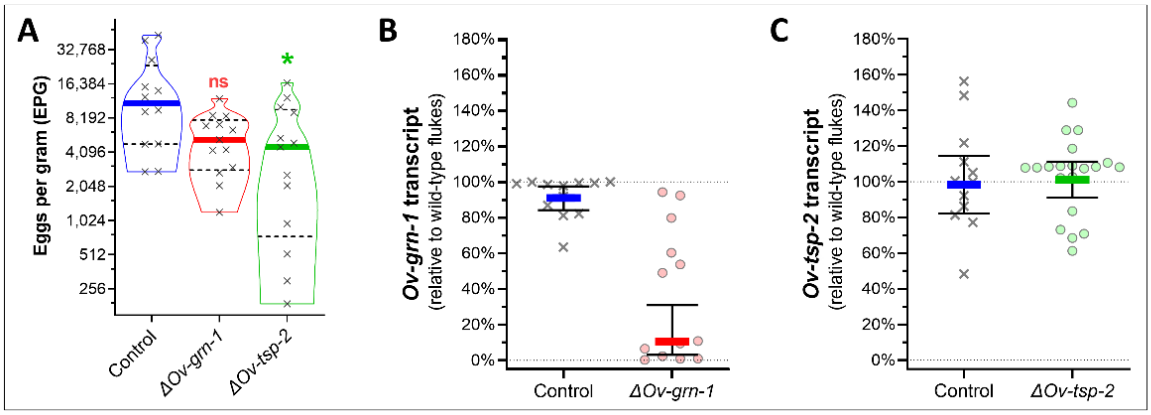

289
290

291 ***Figure 3. Cholangiocarcinoma model, fecundity, gene transcript and mutation rates.*** *Eggs per*
292 *gram of feces (EPG) were assessed at week 23 prior to euthanasia at week 24 (Experiment 2).*
293 *Panel A, EPG values of the three groups of hamsters. Violin plot denotes each hamster's EPG*
294 *with "x" symbols. Solid colored lines indicate the median values and dashed black lines*
295 *indicate the quartiles. Kruskal Wallis with Dunn's multiple comparison correction was used to*
296 *compare EPG levels against control group: *, $P \leq 0.05$; ns, not significant. At necropsy, 12-20*
297 *flukes were sampled from each group, transcript levels determined for Ov-grn-1* ***(B)*** *and Ov-tsp-*
298 *2* ***(C)****, and plotted with each data point representing the transcript level of individual flukes*
299 *relative to wild-type flukes. Resampling with replacement bootstrap analysis (B=1000) of ddCT*
300 *scores (derived from Figure S4) used to generate population average denoted by thick colored*
301 *line and 95% confidence interval error bars.*

302

303 **Synopsis of outcomes of CRISPR/Cas9 gene editing of the liver flukes**

304

305 To characterize mutations from the programmed knockouts, a region of 173 bp flanking the
306 programmed cleavage site in *Ov-grn-1* was scrutinized by analyzing aligned read-pairs from
307 targeted amplicon NGS and analysis of the aligned read-pairs with CRISPResso2 (28).
308 Substitution patterns as determined by the CRISPR-sub tool (29) in the KO groups were not
309 significantly different from the cognate alleles in the controls (Figure S5). Also, we scanned
310 insertions and deletions (indels) and, in turn, the potential impact of indels on the open reading
311 frame. Figure 4A and Table S1 present the indel percentages of juvenile and adult flukes. The
312 *ΔOv-grn-1* pooled NEJs showed 3.26% indel levels (2,723 of 80,571 aligned read-pairs),
313 significantly more than the control group (18 of 51,402 aligned read-pairs, 0.035%) ($P \leq 0.05$).
314 The juvenile and adult flukes in the control group showed similar indel % levels, with 0.045% in
315 the adults (41 of 91,783 aligned read-pairs). Individual *ΔOv-grn-1* adult *O. viverrini* flukes
316 displayed a broad range of editing efficiency in terms of indel profiles. These ranged from an
317 apparent absence of programmed mutation (no indels) to near complete KO (91% indels), with a
318 median of 3.1% indels ($_{M}$*ΔOv-grn-1*), which was significantly higher than in the control group
319 flukes ($P \leq 0.01$). As noted for levels of transcription, however, there were apparently distinct
320 groupings consisting of six low mutation status flukes (termed $_{L}$*ΔOv-grn-1*) and six highly
321 mutation flukes ($_{H}$*ΔOv-grn-1*) observed. From a total of 711 megabase pairs sequenced with 1.7
322 million aligned read pairs, programmed deletions (0.5 million) were overwhelmingly more
323 common than insertions, with only seven insertions identified (Table S1). There was an inverse
324 correlation between efficiency of KO of *Ov-grn-1* (indel percentage) and with a two-tailed non-
325 parametric Spearman correlation co-efficient $r_s = -0.74$ (Figure 4B; $P \leq 0.01$). Only minimal
326 expression of *Ov-grn-1* was detected in the highly mutated, $_{H}$*ΔOv-grn-1* flukes, < 11% level of
327 transcription of control liver flukes. However, the highly edited genotype/highly reduced

328 transcription phenotype contrasted with the wide range of transcription in the flukes with low or
329 moderate levels of editing, $_{L}$*ΔOv-grn-1* and $_{M}$*ΔOv-grn-1,* with a wide range of transcription from
330 6% to 94% of the levels of the control group worms.
331
332 **Evaluation of indel positions**
333
334 With respect to indel length and position, mutations that were detected in the amplicon NGS
335 reads were observed at positions ranging from 29 bp upstream to 54 bp downstream of the
336 double stranded break (DSB+ (ORF nucleotide [nt] position -10 to +74)). Most indels were
337 deletions of a single nucleotide, others were several nucleotides in length, and one of 62 nt was
338 observed. Deletions were noted along the length of the amplicon, with several higher frequency
339 sites indicated with bubbles of greater diameter in Figure 4C. The location of indels in the
340 genomic DNAs pooled from juvenile flukes generally conformed with the location of
341 programmed mutations detected in the genome of the adult stage liver flukes (Figure 4C, large
342 bubbles). Insertions were seen only infrequently but these associated around these high
343 frequency indel locations in juvenile and adult flukes. A cluster of mutations at nucleotide
344 position -1 to -10 bp, within the 5' untranslated region (UTR) of the ORF, was notable given that
345 48 of the 216 indels (22%) observed in adult flukes occurred in this region, and five specific sites
346 included indels detected in the genome of at least seven individual adult worms.
347

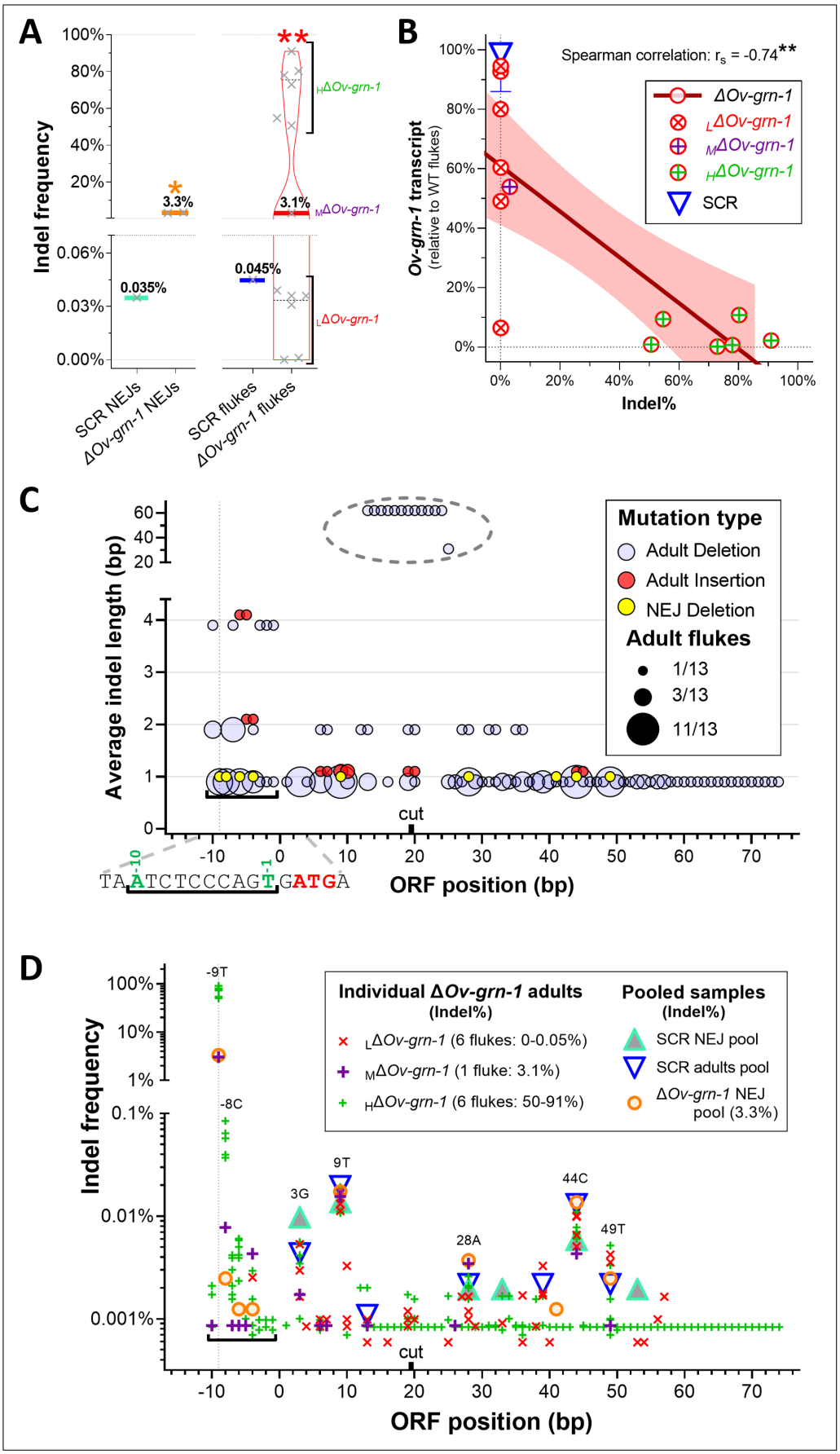
A
Indel frequency
100%
80%
60%
40%
20%
0.06%
0.03%
0.00%
3.3%
3.1%
0.035%
0.045%
**
*
HΔOv-grn-1
MΔOv-grn-1
LΔOv-grn-1
SCR NEJs
ΔOv-grn-1 NEJs
SCR flukes
ΔOv-grn-1 flukes
B
Spearman correlation: rs = -0.74**
Ov-grn-1 transcript
(relative to WT flukes)
Indel%
ΔOv-grn-1
LΔOv-grn-1
MΔOv-grn-1
HΔOv-grn-1
SCR
C
Average indel length (bp)
Mutation type
Adult Deletion
Adult Insertion
NEJ Deletion
Adult flukes
1/13
3/13
11/13
cut
TAATCTCCCAGTGATGA
ORF position (bp)
D
Indel frequency
-9T
-8C
3G
9T
28A
44C
49T
Individual ΔOv-grn-1 adults
(Indel%)
LΔOv-grn-1 (6 flukes: 0-0.05%)
MΔOv-grn-1 (1 fluke: 3.1%)
HΔOv-grn-1 (6 flukes: 50-91%)
Pooled samples
(Indel%)
SCR NEJ pool
SCR adults pool
ΔOv-grn-1 NEJ pool (3.3%)
cut
ORF position (bp)

Figure 4*. Gene mutation rates among liver flukes**. ***A*, Programmed gene knock-out was highly efficient although not in all the flukes. The percentage of total indels (insertions/deletions) determined by next-generation sequencing was plotted on the vertical axis of juvenile and 24 wk adult flukes from Experiment 2. Control group juvenile (NEJ) and adult flukes were each from a single pooled sample while juvenile ΔOv-grn-1 were from pools of two biological replicates s, and ΔOv-grn-1 adults from 13 individual flukes. The highly edited flukes were denoted* $_{H}$*ΔOv-grn-1, flukes with low editing denoted* $_{L}$*ΔOv-grn-1, and the single fluke with median level editing denoted* $_{M}$*ΔOv-grn-1. One sample t-test for either juvenile or adult worms comparing ΔOv-grn-1 and control: *, P ≤ 0.05; **, P ≤ 0.01. The thick solid line is the median and black dashed lines represent the inter-quartiles. A broken Y-axis with a magnified lower portion highlights the near zero values.* ***B.*** *Adult fluke indel mutation rate was inversely correlated with transcript level. The indel and transcript levels were plotted for each individual ΔOv-grn-1 fluke (red circles, combining data from Figures 3C and 4A). Two-tailed non-parametric correlation determined by Spearman co-efficient: **, P ≤ 0.01. For context, the control indel percentages were plotted against the transcript median (blue triangle) with interquartile range error bars.* ***C.*** *ΔOv-grn-1 indel location and size. The NGS reads revealed distinct indel patterns in 12/13 adult flukes. Shown as a multivariate bubble plot, the amplicon base pair open reading frame (ORF position) was plotted against the average indel length. The diameter of the bubbles (1-11) reflected how many of 13 adult flukes recorded a matching indel. The programmed double stranded break between residues 19 and 20 was indicated on the X-axis by the term "cut". For clarity, deletions in adult worm genomes (blue) and insertions (red) have been nudged up/down on the y-axis ±0.1. The deletions in juvenile worms (yellow) are shown from one pooled sample. Insertions were not seen. Position -9 was highlighted with a vertical dotted line and the black horizontal square bracket (└┘) highlighted a cluster of mutations. The sequence around this cluster was shown below the x-axis and the initiator ATG codon indicated in red.* ***D.*** *Mutation rate (indels) at each location: the graph plotted the nucleotide position against the percentage frequency of indels in individual flukes. A vertical dotted line highlighted a mutational hotspot at nucleotide -9 and the black horizontal bracket (└┘) marked a mutational cluster. Other indels of note were labeled with the nucleotide and position.*

348

349 Figure 4D shows the frequency within each sample at each base pair position. There were

350 common locations in the ORF at which both control and *ΔOv-grn-1* juvenile and adults all

351 exhibited a mutation, albeit at low frequency (<0.02%). The location of these indels was denoted

352 with a number/letter to signify the nucleotide position and mutated residue. The cluster of

353 mutations was situated within nucleotide positions -1 to -10 of the 5'UTR of *Ov-grn-1* in adult

354 and juvenile flukes. Similar alleles were not present in the control worms. Although the

355 mutation rate in the 5'-UTR was low overall (<0.09%), numerous mutant alleles were seen at -

356 9T and this single position comprised ~99% of the mutations for the M/H*ΔOv-grn-1* adult and
357 *ΔOv-grn-1* juvenile flukes.
358
359 **Programmed knockout of *Ov-grn-1* impeded malignant transformation**
360
361 Malignant transformation was induced in hamsters by the end point of Experiment 2, at 24 weeks
362 after infection. In the version of the model (7) that we adapted, Syrian hamsters were infected
363 with gene-edited juvenile *O. viverrini* flukes during concurrent exposure to exogenous
364 nitrosamine (Figure 1A). At necropsy, prominent malignant and premalignant lesions of several
365 type were diagnosed frequently in all three treatment groups of hamsters. Figure 5 panels A and
366 B present gross anatomical appearance of livers from representative hamsters, where the CCA
367 was visible to the unaided eye, highlighting the severity of disease that manifested using this
368 model. Specifically, multiple CCA nodules were obvious on both diaphragmatic (Figure 5A) and
369 visceral surfaces (Figure 5B). When micrographs of thin sections of liver were examined,
370 precancerous lesions were evident including biliary dysplasia (a precancerous precursor of CCA
371 (30) in many of the bile ducts and was frequently accompanied by periductal fibrosis (Figure
372 5C). Figure 5 D-F presents representative photomicrographs from each of the treatment groups
373 that highlighted the high-grade, malignant transformation. Figure 5G and Table S2 summarize
374 the findings from the treatment groups. Ten of 12 (83.3%) hamsters in the control group were
375 diagnosed with CCA; high-grade CCA in eight of them and low-grade CCA in other two.
376 Dysplasia also was apparent in the remaining two of the 12 (one mild, one moderate) hamsters in
377 the control group. CCA emerged in seven of 13 hamsters (six with high-grade CCA) in the *ΔOv-*
378 *tsp-2* group. Of the remaining hamsters in this group, two showed mild biliary tract dysplasia,

379 one showed biliary tract proliferation, two exhibited hepatobiliary inflammation, and a single

380 hamster was free of apparent lesions. CAA was diagnosed in nine of 13 in the *ΔOv-grn-1* group,

381 four of which showed high-grade CCA. Of the remaining hamsters, one showed dysplasia, two

382 showed proliferation, and one was free of apparent lesions. Several hamsters infected with *ΔOv-*

383 *tsp-2* (4/13 hamsters) and *ΔOv-grn-1* flukes (3/13 hamsters) exhibited lesions less severe than

384 dysplasia, i.e. inflammation or proliferation, or were free of lesions.

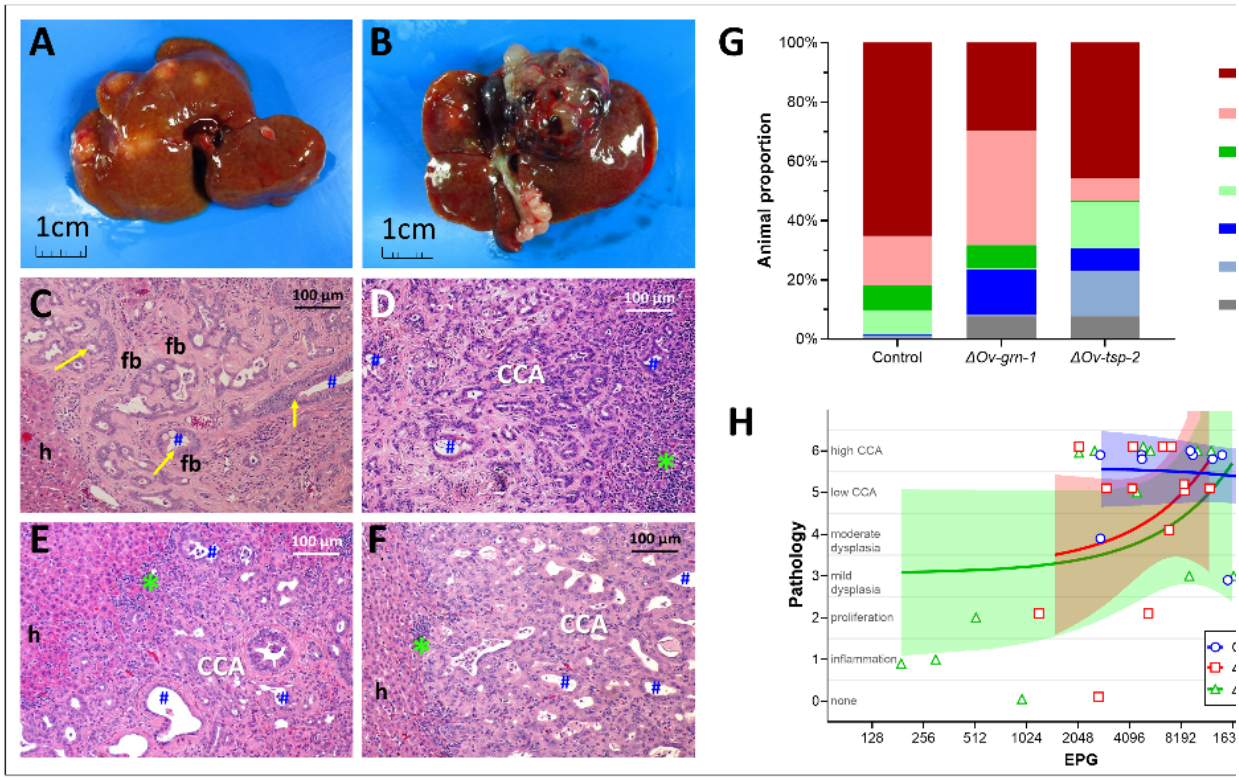

Figure 5. Burden of disease in liver fluke infection associated cholangiocarcinoma*. After resection of the livers at necropsy, a piece of each lobe either fixed in formalin for downstream thin sectioning or was manually disrupted to release flukes, which in turn were examined for gene editing events (Figure 1, Experiment 2). Gross anatomical appearance and histopathological results during induction of cholangiocarcinoma (31) Multiple CCA nodules in the hamster liver presented on both diaphragmatic* ***(A)*** *and visceral surfaces* ***(B)****. Micrographs of H&E-stained thin sections of liver highlighting foci of moderate dysplasia* ***(C)****. This image shows bile ducts (blue #) encircled by dysplastic biliary epithelium (yellow arrow) surrounded by fibrosis (fb) with hepatocytes (h) to the left. H&E stained images of CCA from each of the groups of hamsters group: control* ***(D)****, ΔOv-grn-1* ***(E)****, and ΔOv-tsp-2* ***(F)****. Inflammation marked with green asterisk (*), cholangiocarcinoma labeled as CCA; other labels as in panel C.* ***G.*** *Assessment and scoring of lesions was undertaken independently by*

two co-authors (both veterinary pathologists) using anonymously labeled (blinded) micrographs. The severity of lesions increased from normal tissue (grey) to high grade CCA spanning multiple liver lobes (red). ***H****. EPG from individual hamsters plotted against disease burden on a scale of zero (0, no lesion) to 6 (high CCA) scale. Data plots were slightly reformatted (nudged ± 0.1 on Y-axis) to enable display of overlapping points. Linear regression lines (which were not statistically significant) are shown in shaded color with 95% confidence intervals.*

385

386 Substantial differences were not evident among the treatment groups in the location or subtype of
387 CCA tumors (Table S2). Cholangiocarcinoma mass ranged from microscopic neoplasms with
388 multifocal distributions (12/26) to tumor masses apparent to the unaided eye (14/26) with
389 representative images in Figure 5A, B. With respect to histological classification, 21/26 CCAs
390 were the tubular type, and were seen in the three treatment groups. The papillary/cystic type was
391 seen in a single instance, in an *ΔOv-grn-1* group hamster. Additionally, four mucinous type
392 tumors were observed, one in the control and three in the *ΔOv-tsp-2* group hamsters. The right
393 lobe was the common tumor location (20/26 livers), with nine in the left lobe, and three in the
394 middle lobe. In some cases, tumors had developed in more than one lobe (5/26). Last, we
395 assessed pathology in relation to EPG levels (Figure 5H) and noted there was less disease in
396 *ΔOv-tsp-2* hamsters where EPG was lower, especially in hamsters with EPG < 1,000. However,
397 significant correlation between pathogenesis and EPG was not apparent among the groups.

398

399 **Reduced fibrosis during infection with knockout parasites**

400

401 Hepatic fibrosis was detected in Picro-Sirius Red (PSR)-stained thin tissue sections and enabled
402 investigation and quantification of development of peribiliary fibrosis (Figure 6A). Fibrosis was
403 evaluated, firstly by Ishak staging, a semi-quantitative classification of the degree of fibrosis
404 spread across the liver parenchyma (32) and, secondly, on the fibrotic deposition as

405 demonstrated by staining with PSR localized around the liver flukes, i.e. the amount of collagen
406 deposition surrounding bile ducts occupied where individual liver flukes were situated at the
407 time of necropsy.
408
409 The Ishak scores corresponded to degrees of injurious fibrosis and the levels reflect expansion of
410 fibrosis into periportal regions and the degree of bridging between portal regions, culminating
411 full cirrhosis which is scored as Ishak level 6. The control group was severely affected, with the
412 majority (13/16) of the liver lobes assessed with an Ishak score of 4 (median 4, range 3-4)
413 (Figure 6B). Level 4 indicated that fibrosis had progressed extensively with marked portal-portal
414 and portal-central bridging. Hamsters in the *ΔOv-grn-1* group showed only a single lobe graded
415 at 4 and a majority of lobes (11/17) Ishak grade of 2 (median 2, range 2-4). Level 2 indicated
416 less pathology, with fibrosis in most portal areas with/without short fibrous septa that had not
417 bridged to other portal regions. Hamsters infected with the *ΔOv-tsp-2* liver flukes exhibited
418 similar levels of pathology among the group with Ishak scores ranging from 2 to 4 (median 3).
419 Level 3 was defined as fibrous expansion of most portal areas with occasional bridging among
420 them (32). Periductal fibrosis of the hepatobiliary tract in the *ΔOv-tsp-2* group hamsters was not
421 significantly different in Ishak score from the control group whereas the *ΔOv-grn-1* group
422 displayed significantly less fibrosis than the control ($P \leq 0.001$) or *ΔOv-tsp-2* ($P \leq 0.05$) groups
423 (Figure 6B).

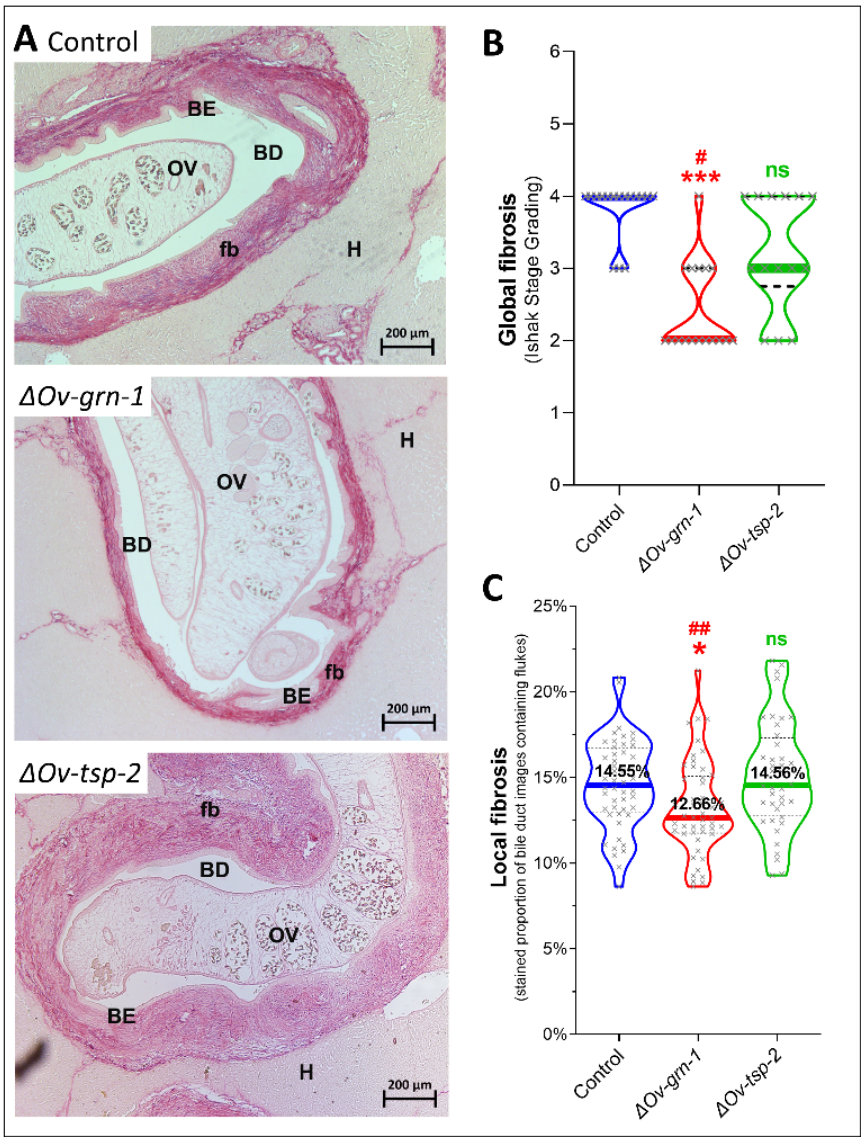

***Figure 6**. **Attenuated liver fibrosis during infection with ΔOv-grn-1 knockout parasites. A.** Representative images of hepatic fibrosis stained by Picro-Sirius Red with CRISPR-Cas9 edited O. viverrini. Fibrosis was denoted as pink/red thick bands around the bile ducts (periductal fibrosis, fb) and expanded from each portal triad with fibrous septa. OV = Opisthorchis viverrini, H = hepatocyte, BD = bile duct, BE = biliary epithelium. **B**. Global liver fibrosis plotted as a violin plot (n = 14-17 liver lobes per group). Livers were scored for fibrosis with an Ishak Stage Grading scale and plotted on a scale spanning from zero (no fibrosis) to six (cirrhosis). **C.** Fibrosis proximal to flukes plotted as a violin plot (n = 46-54 per group). Automated ImageJ fibrosis evaluation of the percentage of collagen deposition in images surrounding fluke-containing bile ducts. Panels B+C: median shown as thick colored line and dashed black lines mark the inter-quartile ranges. Comparing groups with Kruskal-Wallis test with Dunn's multiple comparisons against control: ns =not significant; *, $P \leq 0.05$; ***, $P \leq 0.001$, and against ΔOv-tsp-2 group: #, $P \leq 0.05$; ##, $P \leq 0.01$.*

424 While the Ishak scores showed a significant difference between *ΔOv-grn-1* hamster livers and
425 both other groups, Experiment 1 data showed a higher worm burden in control animals than the
426 gene edited groups, and these extra worms may have contributed to greater fibrosis.
427 Surprisingly, there was no significant correlation between liver fibrosis and EPG for the control
428 or *ΔOv-grn-1* fluke-infected groups, but a significant inverse correlation ($P \leq 0.05$) was detected
429 for the *ΔOv-tsp-2* fluke-infected hamsters (Figure S6). To minimize the impact on fibrosis of
430 different worm burdens, we used automated image analysis to assess periductal fibrosis
431 immediately proximal to liver flukes (which live in the lumen of the bile ducts). An ImageJ
432 driven fibrosis quantification tool for scoring PSR-stained collagen was deployed for automated
433 analysis of the collagen deposition in periductal regions. Of the periductal regions proximal to
434 flukes in the control and the *ΔOv-tsp-2* fluke-infected hamsters, median values of 14.55% (95%
435 CI: 13.6-16.0) and 14.56% (95% CI: 13.5-16.0%) of fibrotic tissue were detected, whereas
436 significantly less (12.66%; 95% CI: 12.1-13.5%) bile duct tissue surrounding *ΔOv-grn-1* flukes
437 was fibrotic (Figure 6C, $P \leq 0.05$). While concerns over worm burden influencing pathology
438 remain, both the control and *ΔOv-tsp-2* group showed very similar localized collagen deposition
439 factors despite very different worm burdens, and suggests that focusing on pathology
440 immediately adjacent to detectable flukes is an accurate and meaningful way to compare
441 pathogenesis on a per worm basis.
442
443 ***Ov-grn-1* KO flukes provoked less cell proliferation**
444

445 Here we explored the *in vivo* effects of programmed knockout of *Ov-grn-1* expression, as
446 opposed to our earlier reports which centered on proliferation of the biliary epithelium and/or
447 cultured cholangiocytes in response to *in vitro* exposure to recombinant *Ov*-GRN-1 (14-17, 33).
448 Proliferation of hamster biliary cells *in situ* was investigated using incorporation of the thymine
449 analogue into cellular DNA. Visualization was performed using immunohistochemistry and
450 evaluated quantitatively (Figure 7A). Concerning worm survival, and its corollary, the fitness
451 cost of the programmed mutation, we examined proliferation but only in the bile ducts where
452 flukes were situated. Median proliferation in bile duct tissue surrounding liver flukes in the
453 control (15.0%, 95% CI: 12.4-22.8%) and *ΔOv-tsp-2* (11.1%, 95% CI: 4.1-20.0%) groups
454 showed wide ranging values but not significantly different from each other (Figure 7B).
455 Whereas the biliary epithelia surrounding *ΔOv-grn-1* flukes showed substantial variation from 0-
456 30%, the majority of the readings were below the other groups with a median of only 3.1% (95%
457 CI: 1.6-7.6%) of cholangiocytes incorporating BrdU ($P \leq 0.001$ vs control; $P \leq 0.05$ vs *ΔOv-tsp-*
458 *2*, Figure 7B). By contrast, the *ΔOv-grn-1* group (3.1%) showed significantly less proliferation
459 than both the control group (4.8-fold reduction, $P \leq 0.001$) and the *ΔOv-tsp-2* group (3.6-fold
460 reduction, $P \leq 0.05$).
461
462 **Mutant *TP53* less frequent during infection with *Ov-grn-1* KO flukes**
463
464 Tumor protein p53 plays a well-recognized role in cholangiocarcinogenesis and is highly
465 expressed in fluke infection associated malignancy (1, 34). A brown nuclear staining pattern
466 presents only in neoplastic biliary cells (Figure 7C). Wide angle images of flukes in the biliary
467 tract showed mutant p53-positive and -negative cells in the epithelium. The profile of p53

468 positive cells differed markedly among the groups: control and *ΔOv-tsp-2* fluke-infected

469 hamsters showed similar levels, 61.1% (95% CI: 43.6-68.3%) and 67.7% (95% CI: 41.5-73.5) of

470 cholangiocytes stained for mutant p53, respectively (Figure 7D). By contrast, of the *ΔOv-grn-1*

471 fluke-infected hamster bile ducts, only 7.5% (95% CI: 2.3-27.5%) exhibited mutant p53-positive

472 cells, ~13% of the levels that manifested in the other groups ($P \leq 0.01$) (Figure 7D).

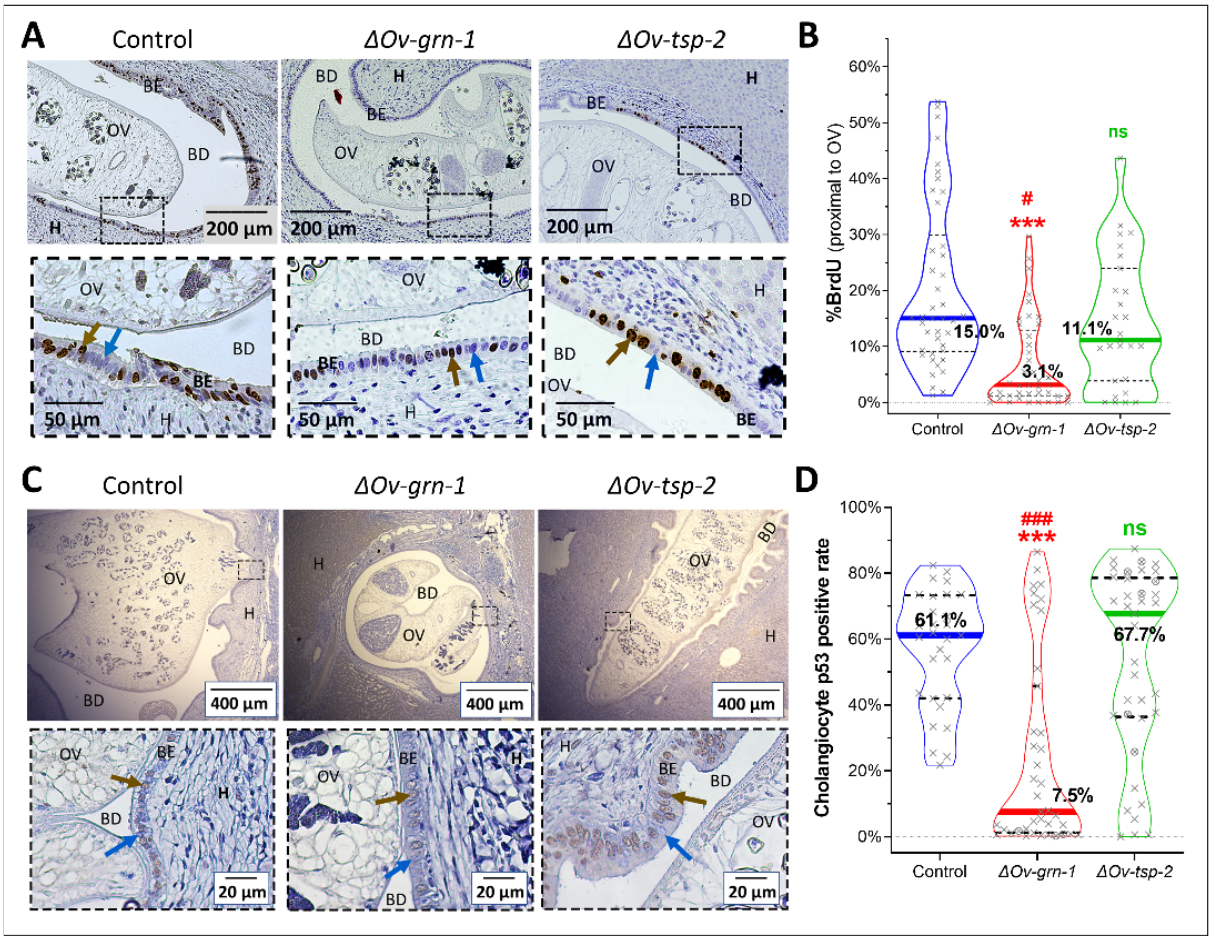

Figure 7. Reduced proliferation and minimal mutant p53 expression in cholangiocytes in hamsters infected with ΔOv-grn-1 genotype liver flukes. *Representative images of biliary cells that incorporated BrdU from regions proximal to flukes in control, ΔOv-grn-1 and ΔOv-tsp-2 groups* ***(A)****. The boxed region in the upper image is magnified in the lower panel. The brown arrow highlights the positive BrdU-stained nuclei and the blue arrow highlights a bile duct cell that did not incorporate BrdU. Violin plots (n = 27-42 per group) of BrdU index measured from cholangiocytes adjacent to where a fluke was located* ***(B)****. Representative micrograph of p53 immunohistochemical staining of biliary epithelium during infection with gene edited flukes* ***(C)****. Anti-mutant p53 antibody stained the nuclei brown (brown arrows); blue arrows indicate negative cells. Black dashed box in upper wide-angle image magnified in*

the lower image to aid visualization. Violin plot (n = 29-39 per group) of mutant p53 positive cholangiocytes as a percentage ***(D)****. When available, 500 to 800 cells were scored from sections of each of the left, middle, and right lobes of the liver marked by "X". Fewer cholangiocytes (300-500) were available for assessment in several samples, denoted by ⓧ Panels A and C: OV = Opisthorchis viverrini, H = hepatocytes, BD = bile duct, BE = biliary epithelium. Panels B, D: non-parametric Kruskal-Wallis test with Dunn's multiple comparison correction compared against control: ns = not significant; ***, P ≤ 0.001, or against ΔOv-tsp-2: #, P ≤ 0.05; ###, P ≤ 0.001. Thick colored lines signify the median and the dashed black lines mark the inter-quartile range.*

Discussion

CCA accounts for ~15% of all primary liver cancers globally and its incidence is increasing (35). Infection with *O. viverrini* is the principal risk factor for CCA in the Lower Mekong River Basin countries including Thailand and Laos PDR, where CCA is the dominant form of liver cancer (1, 22, 36). In an earlier report, we exploited this link to explore the role of *Ov*-GRN-1 secreted by the parasite in tumorigenesis using programmed gene knockout, and reported that the infection was less severe even though gene-edited parasites colonized the biliary tract of hamsters and developed into adult flukes (18). In this follow-up investigation, we report findings during concurrent exposure to dietary nitrosamine and infection with the gene edited parasites, and that KO of the granulin gene retards malignant transformation to CCA, including the emergence of mutant p53, in a rodent model of human opisthorchiasis-associated CCA. These novel results build upon and advance the findings from our original report (18) and, notably, confirmed the role of liver fluke granulin in malignant transformation during chronic opisthorchiasis (15).

We utilized an established model of opisthorchiasis-associated CCA in hamsters that were infected with the parasite during concurrent exposure to exogenous nitrosamine. CCA manifests

491 under these conditions, and this rodent model reflects the human situation where chronic
492 opisthorchiasis in the context of a diet that is rich in fermented fish (in turn, rich in nitrosamines)
493 culminates in a high incidence of CCA (20, 22, 37, 38). In hamsters, opisthorchiasis leads to
494 periductal fibrosis. Chronic periductal fibrosis combined with a nitric oxide carcinogen, such as
495 DMN, results in epithelial cholangiocyte proliferation, hyperplasia, dysplasia, and DNA damage,
496 eventually and reliably manifesting as malignant neoplasia of the biliary tract (20, 21, 39). By
497 contrast, conspicuously less proliferation of the biliary epithelium, reduced mutant p53
498 expression by cholangiocytes, and less periductal fibrosis accompanied infection here with *ΔOv-*
499 *grn-1* genotype worms compared to controls. As noted, our approaches and findings represent a
500 functional genomics (forward genetics)-focused extension of the model pioneered by Thai
501 investigators more than 30 years ago (7).
502
503 Fitness cost of gene knockout can be assessed from programmed gene editing, an approach that
504 is employed for the unbiased identification of essential genes in other organisms and disease
505 settings (40, 41). The present findings confirmed the power of RNA-guided targeted mutation to
506 define essentiality and relevance of two parasite proteins in infection-associated morbidity and
507 malignancy. The *Ov-grn-1* gene does not appear to be essential for *in vivo* development and
508 survival, which has enabled investigation here on the role of this protein in driving cell
509 proliferation, pathology and ultimately contributing to CCA. Nonetheless, the reduced fecundity
510 of *ΔOv-grn-1* liver flukes likely reflected a fitness deficit as the result of the targeted KO. By
511 contrast, *Ov-tsp-2* appears to be essential to parasitism. The *ΔOv-tsp-2* genotype did not survive
512 *in vivo*, and sequencing of the indels across the relevant region of the genome confirmed that
513 most of the surviving flukes from hamsters had not undergone editing at the *Ov-tsp-2* gene locus.

514 These findings build upon earlier RNA interference-mediated silencing of *Ov-tsp-2* gene
515 expression and the resultant malformation of the tegument observed *in vitro* (42). Although
516 infection of hamsters with *Ov-tsp-2* dsRNA-treated parasites was not investigated in this earlier
517 report, the damage to the tegument following exposure to *Ov-tsp-2* dsRNA in worms cultured for
518 several days appeared to be so extensive and debilitating that worms damaged to that extent by
519 either CRISPR-based genome knockout or dsRNA likely did not establish or survive for long
520 periods *in vivo*.
521
522 In *O. viverrini*, *Ov*-GRN-1 and *Ov*-TSP-2 share key, though dissimilar functions at the parasite
523 interface with the mammalian host. *Ov*-GRN-1 induces proliferation of cholangiocytes whereas
524 *Ov*-TSP-2 is a key structural protein of the tegument of liver flukes (and indeed in schistosomes
525 (43, 44)) and of extracellular vesicles that are taken up by host cholangiocytes, among other roles
526 (15, 16, 24). Accordingly, *Ov-tsp-2* was included here as a comparator gene for *Ov-grn-1* KO. A
527 non-targeting guide RNA encoded here by pCas-*Ov*-scramble, also was included, to provide a
528 negative control for off-targeting by the Cas9 nuclease (26). Ultimate lethality of *Ov-tsp-2* KO
529 was borne out in our observation that *ΔOv-tsp-2* genotype flukes failed to survive to the adult
530 stage in the hamsters. Whereas this diminished the value of *ΔOv-tsp-2* worms as controls, the
531 findings highlighted the apparent essentiality of this tetraspanin to the intra-mammalian stages of
532 the liver fluke. This essentiality of tetraspanin contrasted with *Ov*-GRN-1, the absence of which
533 was not lethal to the parasite but which, fortunately, enabled inferences on its contribution to
534 malignant transformation and which reinforced earlier hypotheses on its role as a carcinogen
535 (15). These approaches and findings are novel in the field of functional genomics for helminth
536 parasites and hence, even if targeting *Ov-tsp-2*, in hindsight, was a misstep, the outcome

537 provided a programmed mutation-based demonstration of the essentiality and lethality of
538 mutations of these liver fluke genes, which represents vanguard progress in forward genetics for
539 helminth parasites. Indeed, for context concerning the pioneering significance of this advance,
540 establishing the essentiality of human genes is an active and fertile field in functional genomics
541 and gene therapy (45, 46).
542
543 Notwithstanding that the primary goal of this investigation was to characterize pathogenesis and
544 carcinogenesis associated with infection with *ΔOv-grn-1* flukes in this singular infection/nitroso-
545 compound hamster model, we investigated the mutation profile induced by the CRISPR-based
546 targeted genome editing. Intriguingly, numerous mutations at the targeted *Ov-grn-1* locus were
547 situated within the 5'UTR, rather than in the targeted exon, and most were detected at or
548 proximal to a single residue, referred to here as -9T. This was situated 28 bp 5' to the
549 programmed CRISPR/Cas9 double strand break at nucleotide positions 19 and 20 of the open
550 reading frame. This outcome was unforeseen given that mutations are usually expected at and
551 adjacent to the programmed double stranded break, although guide RNAs have individual, cell-
552 line dependent biases toward particular outcomes (47). The sequence of the 5'UTR of *Ov-grn-1*
553 does not exhibit identity to regulatory elements (UTR database, http://utrdb.ba.itb.cnr.it/), which
554 was unsurprising given that few helminth parasite UTR regulatory elements have been
555 characterized (48). Why this position was preferentially mutated is unclear although the marked
556 reduction of transcription of *Ov-grn-1* that accompanied this mutation profile may signal the
557 presence of a regulatory control element within the UTR.
558

559 Chronic inflammation and fibrosis are risk factors for liver cancer (49). The traditional lifestyle
560 of people living in *O. viverrini*-endemic areas, notably a diet enriched in nitrosamines as well as
561 routine alcohol consumption, in tandem with the assault on the biliary epithelium by the
562 attachment, feeding, movement, and secretions of the liver flukes that result in repeated cycles of
563 injury and repair, establishes a compelling and conducive setting for malignant transformation
564 (5, 50, 51). The secretion of liver fluke granulin into the bile duct and the ability of this growth
565 factor to drive relentless cell proliferation during infection and to (re)heal wounds inflicted by
566 the helminth plays a central role in this process (15). Whereas knockout mutation of *Ov-grn-1*
567 did not prevent development and survival of the liver fluke *in vivo*, infection with these *ΔOv-grn-*
568 *1* flukes failed to lead to marked cell proliferation and fibrosis in the immediate vicinity of the
569 parasites, and consequently fewer hamsters developed high-grade CCA compared with hamsters
570 infected with control and *ΔOv-tsp-2* parasites. Indeed, more hamsters infected with *ΔOv-grn-1*
571 flukes were diagnosed in the categories termed either low-CCA and/or proliferation than in the
572 other two groups. Knockout mutation of *Ov-grn-1* clearly impeded malignant transformation
573 during chronic opisthorchiasis.
574
575 Infected hamsters exhibited elevated rates of *TP53* mutation, however the level was markedly
576 less during infection with *ΔOv-grn-1* flukes. The mutational signatures and related molecular
577 pathways characteristic of human CCAs have been reviewed in depth, and the signature profiles
578 differ between fluke-associated and non-fluke-associated CCAs (1, 34). Fluke-associated CCAs
579 exhibit substantially more somatic mutations than non-fluke related CCAs (34), likely the
580 consequence of opisthorchiasis-associated chronic inflammation. In conformity with the human
581 situation, reduced inflammation and fibrosis were seen during infection with the *ΔOv-grn-1*

582 flukes, further emphasizing the virulence of this growth factor in chronic opisthorchiasis.
583 Inactivating mutations of *TP53* are more prevalent in CCA with a fluke infection etiology, as are
584 mutations of *ARID1A, ARID2*, *BRCA1* and *BRCA2*, than in non-fluke related CCAs (34, 52-55).
585 In addition, hypermethylation has been noted for the promoter CpG islands of several other
586 aberrantly expressed genes (34).
587
588 Mosaicism of gene knock-out is a limitation of our somatic gene-editing approach. Obviating
589 mosaicism by access to transgenic worms following germline transgenesis would clearly be
590 preferable. However, access to transgenic lines of *O. viverrini,* while desirable seems unlikely in
591 the near future, especially considering the genetic complexity of this hermaphroditic
592 platyhelminth obligate parasite with a diploid genome and a multiple host developmental cycle
593 which cannot reliably be established in the laboratory (56). Nonetheless, somatic genome editing
594 is increasingly expedient in the clinic including for the treatment of hemoglobinopathies (57) and
595 the identification of targets for disease intervention in translational medicine (58). Given the role
596 of liver fluke granulin as a virulence factor, the cogent link between CCA and liver fluke
597 infection, and the dismal prospects following a diagnosis of CCA in resource poor settings (1,
598 59, 60), interventions that target this growth factor should be beneficial. Indeed, antibodies raised
599 against liver fluke granulin block its ability to drive proliferation of CCA cell lines (14) and,
600 hence, bootstrap support for a vaccination strategy targeting *Ov*-GRN-1 in the gastro-intestinal
601 tract, for example through induction of mucosal IgA and IgG responses (23, 61). Such an
602 intervention might contribute a productive component to a multivalent, orally administered, anti-
603 infection and anti-cancer vaccine (1, 23), which in turn would augment current tools for the

604 public health intervention and control of this neglected tropical disease and its cancer burden (62,
605 63).
606
607 **Materials and methods**
608
609 **Ethics**
610 The protocol for this research was approved by the Animal Ethics Committee of Khon Kaen
611 University, approval number ACUC-KKU-61/60, which adhered to the guidelines prescribed by
612 the National Research Council of Thailand for the Ethics of Animal Experimentation. All the
613 hamsters were maintained at the animal husbandry facility of the Faculty of Medicine, Khon
614 Kaen University, Khon Kaen.
615
616 **Metacercariae, newly excysted juvenile and adult developmental stages of *O. viverrini***
617
618 Metacercariae (MC) of *O. viverrini* were obtained from naturally infected cyprinid fish
619 purchased from local food markets in the northeastern provinces of Thailand (64). MC were
620 isolated from fishes by using pepsin digestion as described previously (65). Briefly, whole fishes
621 were minced by electric blender and digested with 0.25% pepsin with 1.5% HCl in 0.85% NaCl
622 at 37 ºC for 120 min. The digested fishes were filtered sequentially through sieves of 1100, 350,
623 250, and 140 µm mesh apertures. The filtered, digested tissues were subjected to gravity
624 sedimentation through several changes of 0.85% NaCl until the supernatant was clear.
625 Sedimented MC were identified under a dissecting microscope as *O. viverrini*, and active (i.e.,
626 exhibiting larval movement within the cyst) MC were stored in 0.85% NaCl at 4ºC until used.

627

628 Newly excysted juveniles (NEJ) of *O. viverrini* were induced to escape from the metacercarial
629 cyst by incubation in 0.25% trypsin in PBS supplemented with 2× 200 U/ml penicillin, 200
630 µg/ml streptomycin (2× Pen/Strep) for 5 min at 37°C in 5% CO_2 in air. The juvenile flukes were
631 isolated free of discarded cyst walls by mechanical passage through a 22 G needle (18). We also
632 use the term NEJ for the juvenile flukes because NEJ is also widely used for juveniles of related
633 liver flukes (66, 67).

634

635 **Plasmid constructs and transfection of *O. viverrini***

636

637 The CRISPR plasmid encoding a guide RNA (gRNA) complimentary to *Ov-grn-1* exon 1 termed
638 pCas-*Ov-grn-1* was constructed using the GeneArt CRISPR Nuclease Vector kit (Thermo Fisher
639 Scientific), as described . The programmed cleavage site at nucleotide position 1589–1608, 5'-
640 GATTCATCTACAAGTGTTGA with a CGG proto-spacer adjacent motif (PAM) which
641 determined the cleavage site located at three nucleotides upstream on *Ov-grn-1* was designed
642 using the online tools, http://crispr.mit.edu/ (68) and CHOPCHOP,
643 http://chopchop.cbu.uib.no/ (69, 70) using the *Ov-grn-1* gene (6,287 bp, GenBank FJ436341.1)
644 as the reference. A second plasmid, termed pCas-*Ov-tsp-2* was constructed using the same
645 approach; pCas-*Ov-tsp-2* encodes a gRNA targeting exon 5 of the *Ov-tsp-2* gene (10,424 bp,
646 GenBank JQ678707.1) (71, 72). The guide RNAs encoded by *Ov-grn-1* and *Ov-tsp-2* exhibited
647 theoretically high, on-target efficiency and little or no off-target matches to the *O. viverrini*
648 genome. A third construct, termed pCas-*Ov*-scramble was also prepared and included as a
649 control to normalize analysis of gene expression and programmed gene knockout. The pCas-*Ov-*

650 scramble construct included as the gRNA, a transcript of 20 nt, 5'-
651 GCACTACCAGAGCTAACTCA which exhibits only minimal identity to the *O. viverrini*
652 genome and which lacks a PAM (73). A non-targeting guide RNA (26), encoded here by pCas-
653 *Ov*-scramble, provided a negative control for off-targeting by the Cas9 nuclease. A mammalian
654 U6 promoter drives transcription of the gRNAs in all three plasmids and the CMV promoter
655 drives expression of the *Streptococcus pyogenes* Cas9 nuclease, modified to include the
656 eukaryotic nuclear localization signals 1 and 2. To confirm the orientation and sequences of
657 gRNA in the plasmid vector, *Escherichia coli* competent cells (TOP10) were transformed with
658 the plasmids, plasmid DNAs were recovered from ampicillin resistant colonies using a kit
659 (NucleoBond Xtra Midi, Macherey-Nagel GmbH, Düren, Germany), and the nucleotide
660 sequences of each construct confirmed as correct by Sanger direct cycle sequencing using a U6-
661 specific sequencing primer.
662
663 Two hundred juvenile *O. viverrini* were dispensed into an electroporation cuvette, 4 mm gap
664 (Bio-Rad, Hercules, CA) containing 20 µg pCas-*Ov-grn-1,* pCas-*Ov-tsp-2* or pCas-*Ov*-scramble
665 in a total volume of 500 µl RPMI, and subjected to a single square wave pulse at 125 V for 20
666 ms (Gene Pulser Xcell, Bio-Rad). These juvenile flukes were maintained in culture in RPMI
667 supplemented with 1% glucose for 60 min after which they were used for infection of hamsters
668 by stomach gavage (below).
669
670 **Infection of hamsters with gene edited *O. viverrini* juveniles**
671

672 Wild-type (WT) flukes were collected and prepared for qPCR from infected hamsters 8 weeks
673 after infection as previously described . Figure 1 provides a timeline of the CCA model,
674 employed in Experiments 1 and 2. In Experiment 1, nine male hamsters (Syrian golden hamster,
675 *Mesocricetus auratus*) aged between 6-8 weeks were randomly divided into three experimental
676 groups (Figure 1). Each hamster was infected with 100 *O. viverrini* NEJs by gastric gavage.
677 These juvenile flukes had been transfected with pCas-*Ov-grn-1* plasmid, pCas-*Ov-tsp-2*, or the
678 control pCas-*Ov*-scramble, and assigned the following identifiers: delta(Δ)-*gene* name, *ΔOv-grn-*
679 *1, ΔOv-tsp-2,* or control, respectively. The infected hamsters were maintained under a standard
680 light cycle (12 hours dark/light) with access to water and food *ad libitum*. Two weeks following
681 infection, the drinking water provided to hamsters was supplemented with dimethylnitrosamine
682 (DMN) (synonym, *N*-nitrosodimethylamine) (Sigma-Aldrich, Inc., St. Louis, MO) at 12.5 ppm
683 until 10 weeks following infection (7, 19, 20). Feces from each hamster were collected for fecal
684 egg counts at weeks 10 and 12 after infection. The hamsters were euthanized at week 14 by
685 inhalation overdose of isoflurane, followed by removal of the liver. Liver flukes were recovered
686 from the liver, counted, and prepared for qPCR analysis of targeted genes.
687
688 In Experiment 2, 45 male hamsters, 6–8 weeks of age, were randomly divided into three groups
689 each with 15 hamsters and infected with gene edited NEJs and DMN added to drinking water (as
690 in Experiment 1). Hamster feces were collected at week 23 after infection for fecal egg counts.
691 At week 24, 40 mg/kg thymine analogue 5-bromo-2'-deoxyuridine (BrdU, Abcam, College
692 Science Park, UK) was introduced into the peritoneum at 30 min before euthanasia, for
693 incorporation into the nuclei for investigation of proliferation of the biliary epithelia (74).
694 Hamsters were euthanized, the liver resected from each hamster, the liver lobes separated, and

695 the left, middle and right lobes fixed in 10% formalin. We used a shorthand to label the lobes:
696 left (left dorsocaudal), middle (combined ventral and dorsal median lobes), and right (right
697 dorsocaudal). Liver flukes that were incidentally released from bile ducts during liver
698 preparation and o fixation for thin sectioning were retained and stored in RNAlater (Thermo
699 Fisher). Levels of gene expression, mutation efficiency, and mutation profile were assessed in
700 this sample of the liver flukes.
701
702 **Histopathological investigation**
703
704 From each hamster, the entire liver was dissected and immersed in 10% buffered formalin. After
705 overnight fixation, the liver lobes were processed for embedding in paraffin by dehydration
706 through series of a 70%, 90%, and 100% ethanol, cleared in xylene, subjected to infiltration by
707 paraffin at 56°C, and last, embedding in paraffin. Four μm sections were sliced by microtome
708 from the paraffin-embedded liver, the sections stained with hematoxylin and eosin (H&E).
709 Histopathological grading was undertaken by examination of the stained sections of liver and
710 bile duct for inflammation, bile duct changes, dysplasia (including dysplasia in
711 cholangiofibrosis), and stage of CCA as described (21, 75-77), with modifications (Table 1).
712
713
714
715
716
717
718

719 **Table 1**. Criteria for histopathological and histochemical assessment and grading.
720
721

Histopathological lesion	Grade description	Reference
Inflammation	0 = None (no/minimal liver tissue or portal inflammation) 1 = Mild (1-2 foci per 4× objective at hepatocyte & periportal area) 2 = Moderate (3-5 foci per 4× objective at hepatocyte & periportal area) 3 = Severe (> 5 foci per 4× objective at hepatocyte & periportal area)	(21, 77, 78)
Bile duct changes	0 = None (absence of proliferation and cholangiofibrosis) 1 = Mild (bile duct proliferation without cholangiofibrosis or periductal fibrosis) 2 = Moderate (bile duct proliferation with cholangiofibrosis) 3 = Severe (bile duct proliferation with cholangiofibrosis and periductal fibrosis)	(21, 77, 78)
Dysplasia	0 = None (No cellular atypia, no nuclear polarity, no nuclear protrusions, no nuclear pseudostratification) 1 = Mild (Cellular atypia+, no nuclear polarity, no nuclear protrusions, nuclear pseudostratification+, nuclei within the lower two-thirds) 2 = Moderate (Cellular atypia+, nuclear polarity+, protruding of nuclei+, nuclear pseudostratification+) 3 = High (Cellular atypia++, nuclear polarity++, protruding of nuclei+, nuclear pseudostratification+)	(76)
Cholangiocarcinoma	0 = None (no evidence of CCA) Low CCA: 1 = Mild (CCA area 1-2 foci per 4× objective) High CCA: combined 2+3: 2 = Moderate (CCA area 3-5 foci per 4× objective) and 3 = Severe (CCA area> 5 foci per 4× objective)	(21, 77, 78)
Fibrosis (PSR stain):	0 =No fibrosis	(32, 79)

Ishak score	1 = Fibrous expansion of some portal areas, with or without short fibrous septa 2 = Fibrous expansion of most portal areas, with or without short fibrous septa 3 = Fibrous expansion of most portal areas with occasional portal to portal bridging 4 = Fibrous expansion of portal areas with marked bridging; portal to portal as well as portal to central 5 = Marked bridging (portal–portal and/or portal–central) with occasional nodules (incomplete cirrhosis) 6 = Cirrhosis, probable or definite	
Assessment of collagen proximal to liver flukes	Quantitative automated evaluation of collagen deposition percentage surrounding bile ducts	ImageJ MRI Fibrosis Tool BioCampus, Montpellier, France (Volker Bäcker 2015), www.mri.cnrs.fr https://dev.mri.cnrs.fr/projects/imagej-macros/wiki/Fibrosis_Tool

722
723

724 **Fecal egg counts and worm counts**

725

726 Feces from each hamster were individually collected, weighed and *O. viverrini* eggs per gram of
727 feces (EPG) calculated using a modified formalin-ethyl acetate technique (80). In brief, hamster
728 feces were collected and fixed in 10 ml of 10% formalin. Thereafter, the slurry of formalin-fixed
729 feces was filtered through two layers of gauze, and clarified by centrifugation at 500 *g* for 2 min.
730 The pellet was resuspended with 7 ml of 10% formalin, mixed with 3 ml ethyl-acetate and
731 pelleted at 500 *g* for 5 min. The pellet was resuspended in 10% formalin solution and examined
732 at 400× by light microscopy. EPG was calculated as follows: (average number eggs × total drops
733 of fecal solution)/ gram of feces. To recover the adult liver flukes, food was withdrawn from the

734 hamsters 16 hours before euthanasia. Intact mature *O. viverrini* from the hepatobiliary tract were
735 recovered during observation of the livers using a stereo dissecting microscope and stored for
736 downstream gene-editing investigation.
737
738 **Extraction of nucleic acids**
739
740 Pooled NEJ or single mature worms from either experimental or control groups were
741 homogenized in RNAzol RT (Molecular Research Center, Inc., Cincinnati, OH) before dual
742 RNA and DNA extraction as described . Briefly, the parasite(s) were homogenized in RNAzol
743 RT using a motorized pestle, after which the DNA and protein were precipitated in nuclease free
744 water. The aqueous upper phase was transferred into a new tube for total RNA precipitation by
745 isopropanol (50% v/v). The DNA/protein pellet was resuspended in DNAzol and genomic DNA
746 extracted according to the manufacturer's instructions (Molecular Research Center).
747 Concentration and integrity of genomic DNA and total RNA were independently quantified by
748 spectrophotometry (NanoDrop 1000, Thermo Fisher, Waltham, MA). Transcription and
749 expression were investigated in pools of NEJs and in individual adult flukes after normalization
750 against the controls.

751 **Quantitative real-time PCR**

752 cDNA was synthesized from DNase I-treated-total RNA (10 ng) using Maxima First Strand
753 cDNA synthesis with a DNase kit (Thermo Scientific) prior to performing quantitative real-time
754 PCR (qPCR). Each cDNA sample was prepared for qPCR in triplicate using SSoAdvanced
755 Universal SYBR Green Supermix (Bio-Rad). Each qPCR reaction consisted of 5 µl of SYBR
756 Green Supermix, 0.2 µl (10 µM) each of specific forward and reverse primers for *Ov-grn-1*

757 (forward primer, *Ov*-GRN-1-RT-F: 5'-GACTTGTTGTCGCGGCTTAC-3' and reverse
758 primer, *Ov*-GRN1-RT-R: 5'-CGCGAAAGTAGCTTGTGGTC-3'), amplifying 147 base pairs
759 (bp) of 444 nt of *Ov-grn-1* mRNA, complete cds GenBank FJ436341.1) or primers for *Ov-tsp-2*
760 (forward primer, *Ov-TSP-2*-F 5'- ACAAGTCGTATGTGGAATCA- 3' and reverse primer *Ov-*
761 *TSP-2*-R 5'- CCGTCTCGCCTTCTCCTTT- 3', product size 377 bp of 672 nt of *Ov-tsp-2*A
762 mRNA, complete cds (GenBank JQ678707.1), 2 µl of cDNA and distilled water to a final
763 volume of 10 µl were used in the reaction. The thermal cycle was a single initiation cycle at
764 95°C for 10 min followed by 40 cycles of denaturation at 95°C for 15s, annealing at 55°C for 30s
765 using CFX Connect Real-Time PCR system (Bio-Rad). The endogenous actin gene (1301 nt of
766 *Ov-actin* mRNA, GenBank EL620339.1) was used as a reference (17, 81, 82) (forward
767 primer, *Ov*-actin-F: 5'-AGCCAACCGAGAGAAGATGA and reverse primer, *Ov*-actin-R: 5'-
768 ACCTGACCATCAGGCAGTTC. The fold change in *Ov-grn-1* and *Ov-tsp*-2 transcripts was
769 calculated using the $2^{(-\Delta\Delta Ct)}$ method using the *Ov-actin* gene as a reference for normalization (17,
770 81, 82). Transcript ddCT qPCR data were resampled with replacement bootstrap analysis in
771 Microsoft Excel with 1000 bootstrap resamples (B = 1000, n = original sample number) to
772 generate mean values and 95% confidence intervals (83).
773
774 **Illumina based targeted next generation sequencing of targeted amplicons**
775
776 The Amplicon-EZ next generation sequencing service (GENEWIZ, South Plainfield, NJ) was
777 used to obtain deeper coverage of *Ov-grn-1* exon 1 from individual mature worms or pooled
778 NEJ, providing > 50,000 complete amplicon aligned read-pairs per sample. A 173-nucleotide
779 region flanking the programmed DSB was amplified with forward primer 5'-

780 TTCGAGATTCGGTCAGCCG-3' and reverse primer 5'-GCACCAACTCGCAACTTACA-3',
781 and was sequenced directly using Illumina chemistry. The CRISPR RGEN Tool web platform
782 (http://www.rgenome.net/about/) analysis, comparison range 60 nt, was used to screen for Cas9-
783 catalyzed substitutions in the aligned read-pairs with comparisons among the treatment groups
784 (84, 85). In addition, CRISPResso2 with a quantification window set at 30 nt (28) was employed
785 for indel estimation, as described (18). The NGS reads are available at GenBank Bioproject
786 PRJNA385864, BioSample SAMN07287348, SRA study PRJNA385864, accessions SRR
787 15906234-15906251.
788
789 **BrdU-staining for proliferation of the biliary epithelium**
790
791 Proliferation of biliary epithelial cells was investigated by using incorporation of BrdU. In brief,
792 the liver sections of a paraffin-embedded sample were soaked in xylene, rehydrated in graded
793 alcohol solution (100%, 90%, and 70% ethanol for 5 min each), and antigen was retrieved in
794 citrate buffer (pH 6) for 5 min in a high-pressure cooker. The tissue sections were blocked with
795 3% H_2O_2 in methanol for 30 min and subsequently incubated with 5% fetal bovine serum in
796 phosphate buffered saline for 30 min at room temperature (RT). The sections were incubated
797 with monoclonal mouse anti-BrdU (Abcam, catalogue no. ab8955) diluted 1:200 in PBS at 4°C
798 overnight, and then probed with goat anti-mouse IgG-HRP (Invitrogen, Thermo Fisher) diluted
799 1:1,000 in PBS for 60 min at RT. The peroxidase reaction was developed with 3, 3'-
800 diaminobenzidine (DAB). Sections were counterstained with Mayer's hematoxylin for 5 min
801 before dehydrating and mounting. A positive signal was indicated by a brown color under light
802 microscopy. The image was captured by a Zeiss Axiocam microscope camera ICc5 and NIS-

803 Element software (Nikon, Minato, Tokyo, Japan). To quantify BrdU-positive nuclei,
804 cholangiocytes were counted in 10 non-overlapping fields of 400x magnification, with a total of
805 1,000 biliary cholangiocytes counted using the counter plug-in tool at ImageJ 1.52P. The cell
806 proliferation index was calculated as a percentage using the formula: positive biliary nuclei/total
807 biliary cells x100%.
808
809 **Staining for mutant forms of p53**
810
811 To investigate levels of p53 mutation (86) in cholangiocytes, paraffin-embedded tissue sections
812 were deparaffinized and rehydrated by standard methods. Thereafter, sections were incubated
813 with monoclonal mouse anti-p53 (mutant, clone Ab-3 PAb240 catalogue no. OP29-200UG)
814 (Merck, Darmstadt, Germany) diluted 1:100 in PBS at 4°C overnight, and after thorough
815 washing, probed with goat anti-mouse IgG-HRP (Invitrogen, Carlsbad, CA) diluted 1:1,000 in
816 PBS for 60 min at 25°C. The peroxidase reaction was developed with 3,3'- DAB and sections
817 counterstained with Mayer's hematoxylin for 5 min. A human CCA cell line served as the
818 positive control for p53 positivity (87, 88). Images of high-power fields (400x magnification) of
819 the biliary epithelium were taken in five non-overlapping fields of each of the right, middle, and
820 left liver lobes using a Zeiss Axiocam fitted with a ICc5 camera and NIS-Element software
821 (Nikon). The percentage of mutant p53-positive cholangiocytes was determined by calculating
822 positive cells from 500 to 800 cholangiocytes from the right, middle, and left lobes of the liver
823 using imageJ.
824
825 **PSR staining to evaluate fibrosis**

826

827 Liver tissue sections where *O. viverrini* reside were selected for fibrosis measurements with PSR
828 (Abcam, catalogue ab150681). The thin sections were deparaffinized in xylene and rehydrated
829 through an ethanol gradient. PSR solution was applied to the sections and incubated at 25°C for
830 60 min. Excess dye was removed by washing twice in dilute acetic acid (0.5%) after which
831 sections were dehydrated through graded series of ethanol and xylene, the slides cleared with
832 100% xylene, mounted in Per-mount, and air dried overnight. Fibrosis surrounding the bile duct
833 (periductal fibrosis, PF) proximal to the liver flukes was evaluated by two approaches. First, by
834 scoring according to accepted criteria (32): samples were blinded and fibrosis scores (0-6) were
835 graded semi-quantitatively by Ishak stage (Table 1) by two experienced pathologists. Second,
836 localized fibrosis was evaluated by capturing images for quantification of collagen deposition.
837 Specifically, the PSR-stained fibrotic lesions was measured using the plug-in fibrosis tool
838 developed by Volker Bäcker (New FUJI toolsets for bioimage analysis, available at
839 https://github.com/MontpellierRessourcesImagerie/imagej_macros_and_scripts/wiki/MRI_Fibro
840 sis_Tool. We (18) and others (89, 90) have previously used this tool with PSR-stained tissues.
841

842 **Statistical analysis**

843

844 One-way ANOVA with Tukey multiple comparisons was used for comparisons with two to four
845 replicates (worm burden and EPG at week 14). The Krustal-Wallis non parametric test with
846 Dunn's multiple comparisons was used for datasets that were not normally distributed including
847 the 24-week EPGs, Ishak and periductal fibrosis, BrdU scores, and mutant p53 signals.
848 Replicates and errors bars are as listed in each figure legend. Statistical analysis and graphic

849 presentation of the results were undertaken using GraphPad Prism version 9 (GraphPad Software
850 Inc, San Diego, CA). To compare mutation rate, a one sample *t*-test compared the replicate
851 %indel values for the *ΔOv-grn-1* against the single control group % indel for either juvenile or
852 adult *O. viverrini* worms. Assessment for correlation between % indel and transcription was
853 carried out using a two-tailed non-parametric Spearman correlation co-efficient (r_s). Values of P
854 ≤ 0.05 were considered to be statistically significant: an asterisk (*) corresponds to the control vs
855 *ΔOv-grn-1* group comparison; *, $P \leq 0.05$, **, $P \leq 0.01$, ***, $P \leq 0.001$, hashtag (#) for *ΔOv-grn-*
856 *1* vs *ΔOv-tsp-2* group comparison; #, $P \leq 0.05$; ##, $P \leq 0.01$; ###, $P \leq 0.001$.
857

858 **Acknowledgements**

859

860 We thank Suwit Balthaisong for technical assistance. This study was supported by the Research
861 Program, Research and Graduate Studies, Khon Kaen University to SC, ST and TL, the National
862 Cancer Institute, National Institutes of Health (NIH) USA award R01CA164719 (AL, TL, PJB,)
863 and the Australian National Health and Medical Research Council, NHMRC award APP1085309
864 to AL, JS and TL, and senior principal research fellowship APP1117504 to AL. This research
865 was funded in part, by the Wellcome Trust, grant number 107475/Z/15/Z to PJB. For the purpose
866 of Open Access, the authors have applied a CC BY public copyright license to any Author
867 Accepted Manuscript version arising from this submission. The funders had no role in the study
868 design, data collection and analysis, decision to publish, and/or preparation of the manuscript.
869 The content is solely the responsibility of the authors and does not necessarily represent the
870 official views of the NCI, NIH, NHMRC, or WT.
871

872 **Author contributions**

873

874 T. Laha, A. Loukas, P. Brindley, S. Tangkawattana, S. Chaiyadet, W. Ittiprasert, P. Arunsan, and
875 M. Smout conceived and designed the research; S. Chaiyadet, S. Tangkawattana, R. Deenonpoe,
876 V. Mann, M. Smout, and W. Ittiprasert performed the research; S. Chaiyadet, S. Tangkawattana,
877 R. Deenonpoe, and M. Smout recorded the findings ; T. Laha, P.J. Brindley, A. Loukas, M.
878 Smout and W. Ittiprasert contributed reagents and analytical tools; T. Laha, S. Chaiyadet, P.
879 Arunsan, S. Tangkawattana, V. Mann, M. Smout, and W. Ittiprasert completed the experiments;
880 S. Chaiyadet, S. Tangkawattana, W. Ittiprasert, and M. Smout analyzed data; S. Chaiyadet, S.
881 Tangkawattana, T. Laha, P. Brindley, W. Ittiprasert, M. Smout, and A. Loukas prepared figures
882 and wrote the paper.

883 **Author ORCiD**

884 Wannaporn Ittiprasert, http://orcid.org/0000-0001-9411-8883
885 Michael J. Smout, https://orcid.org/0000-0001-6937-0112
886 Paul J. Brindley, https://orcid.org/0000-0003-1765-0002
887 Alex Loukas, https://orcid.org/0000-0002-0896-8441

888

889 **Conflict of interest**. The authors declare that this study was performed without any commercial
890 or financial relationships construable as potential conflicts of interest.

891
892
893 **References**
894

895 1. Brindley PJ, Bachini M, Ilyas SI, Khan SA, Loukas A, Sirica AE, et al.
896 Cholangiocarcinoma. Nat Rev Dis Primers. 2021;7(1):65.

897 2. Fedorova OS, Kovshirina AE, Kovshirina YV, Hattendorf J, Onishchenko SV,
898 Katanakhova LL, et al. Opisthorchis felineus infection is a risk factor for cholangiocarcinoma in
899 Western Siberia: a hospital-based case-control study. Clin Infect Dis. 2022.
900 3. IARC. Biological agents. Volume 100 B. A review of human carcinogens. IARC
901 monographs on the evaluation of carcinogenic risks to humans. 2012;100(Pt B):1-441.
902 4. Brindley PJ, da Costa JM, Sripa B. Why does infection with some helminths cause
903 cancer? Trends Cancer. 2015;1(3):174-82.
904 5. Sripa B, Brindley PJ, Mulvenna J, Laha T, Smout MJ, Mairiang E, et al. The tumorigenic
905 liver fluke Opisthorchis viverrini--multiple pathways to cancer. Trends Parasitol.
906 2012;28(10):395-407.
907 6. Shin HR, Oh JK, Masuyer E, Curado MP, Bouvard V, Fang YY, et al. Epidemiology of
908 cholangiocarcinoma: an update focusing on risk factors. Cancer Sci. 2010;101(3):579-85.
909 7. Thamavit W, Kongkanuntn R, Tiwawech D, Moore MA. Level of Opisthorchis
910 infestation and carcinogen dose-dependence of cholangiocarcinoma induction in Syrian golden
911 hamsters. Virchows Arch B Cell Pathol Incl Mol Pathol. 1987;54(1):52-8.
912 8. Srivatanakul P, Ohshima H, Khlat M, Parkin M, Sukaryodhin S, Brouet I, et al.
913 Opisthorchis viverrini infestation and endogenous nitrosamines as risk factors for
914 cholangiocarcinoma in Thailand. Int J Cancer. 1991;48(6):821-5.
915 9. Sriraj P, Boonmars T, Aukkanimart R, Songsri J, Sripan P, Ratanasuwan P, et al. A
916 combination of liver fluke infection and traditional northeastern Thai foods associated with
917 cholangiocarcinoma development. Parasitol Res. 2016;115(10):3843-52.
918 10. Thamavit W, Ngamying M, Boonpucknavig V, Boonpucknavig S, Moore MA.
919 Enhancement of DEN-induced hepatocellular nodule development by Opisthorchis viverrini
920 infection in Syrian golden hamsters. Carcinogenesis. 1987;8(9):1351-3.
921 11. Maizels RM, Smits HH, McSorley HJ. Modulation of Host Immunity by Helminths: The
922 Expanding Repertoire of Parasite Effector Molecules. Immunity. 2018;49(5):801-18.
923 12. Drurey C, Maizels RM. Helminth extracellular vesicles: Interactions with the host
924 immune system. Mol Immunol. 2021;137:124-33.
925 13. Brindley PJ, Loukas A. Helminth infection-induced malignancy. PLoS Pathog.
926 2017;13(7):e1006393.
927 14. Smout MJ, Laha T, Mulvenna J, Sripa B, Suttiprapa S, Jones A, et al. A granulin-like
928 growth factor secreted by the carcinogenic liver fluke, Opisthorchis viverrini, promotes
929 proliferation of host cells. PLoS Pathog. 2009;5(10):e1000611.
930 15. Smout MJ, Sotillo J, Laha T, Papatpremsiri A, Rinaldi G, Pimenta RN, et al.
931 Carcinogenic Parasite Secretes Growth Factor That Accelerates Wound Healing and Potentially
932 Promotes Neoplasia. PLoS Pathog. 2015;11(10):e1005209.
933 16. Haugen B, Karinshak SE, Mann VH, Popratiloff A, Loukas A, Brindley PJ, et al.
934 Granulin Secreted by the Food-Borne Liver Fluke Opisthorchis viverrini Promotes Angiogenesis
935 in Human Endothelial Cells. Front Med (Lausanne). 2018;5:30.
936 17. Papatpremsiri A, Smout MJ, Loukas A, Brindley PJ, Sripa B, Laha T. Suppression of Ov-
937 grn-1 encoding granulin of Opisthorchis viverrini inhibits proliferation of biliary epithelial cells.
938 Exp Parasitol. 2015;148:17-23.
939 18. Arunsan P, Ittiprasert W, Smout MJ, Cochran CJ, Mann VH, Chaiyadet S, et al.
940 Programmed knockout mutation of liver fluke granulin attenuates virulence of infection-induced
941 hepatobiliary morbidity. Elife. 2019;8:e41463.

942 19. Loilome W, Yongvanit P, Wongkham C, Tepsiri N, Sripa B, Sithithaworn P, et al.
943 Altered gene expression in Opisthorchis viverrini-associated cholangiocarcinoma in hamster
944 model. Molecular carcinogenesis. 2006;45(5):279-87.
945 20. Thamavit W, Pairojkul C, Tiwawech D, Shirai T, Ito N. Strong promoting effect of
946 Opisthorchis viverrini infection on dimethylnitrosamine-initiated hamster liver. Cancer Lett.
947 1994;78(1-3):121-5.
948 21. Lvova MN, Tangkawattana S, Balthaisong S, Katokhin AV, Mordvinov VA, Sripa B.
949 Comparative histopathology of Opisthorchis felineus and Opisthorchis viverrini in a hamster
950 model: an implication of high pathogenicity of the European liver fluke. Parasitol Int.
951 2012;61(1):167-72.
952 22. Sripa B, Kaewkes S, Sithithaworn P, Mairiang E, Laha T, Smout M, et al. Liver fluke
953 induces cholangiocarcinoma. PLoS Med. 2007;4(7):e201.
954 23. Phumrattanaprapin W, Chaiyadet S, Brindley PJ, Pearson M, Smout MJ, Loukas A, et al.
955 Orally Administered Bacillus Spores Expressing an Extracellular Vesicle-Derived Tetraspanin
956 Protect Hamsters Against Challenge Infection With Carcinogenic Human Liver Fluke. J Infect
957 Dis. 2021;223(8):1445-55.
958 24. Suttiprapa S, Sotillo J, Smout M, Suyapoh W, Chaiyadet S, Tripathi T, et al. Opisthorchis
959 viverrini Proteome and Host-Parasite Interactions. Adv Parasitol. 2018;102:45-72.
960 25. Chaiyadet S, Sotillo J, Krueajampa W, Thongsen S, Smout M, Brindley PJ, et al.
961 Silencing of Opisthorchis viverrini Tetraspanin Gene Expression Results in Reduced Secretion
962 of Extracellular Vesicles. Front Cell Infect Microbiol. 2022;12:827521.
963 26. Morgens DW, Wainberg M, Boyle EA, Ursu O, Araya CL, Tsui CK, et al. Genome-scale
964 measurement of off-target activity using Cas9 toxicity in high-throughput screens. Nat Commun.
965 2017;8:15178.
966 27. Sithithaworn P, Tesana S, Pipitgool V, Kaewkes S, Pairojkul C, Sripa B, et al.
967 Relationship between faecal egg count and worm burden of Opisthorchis viverrini in human
968 autopsy cases. Parasitology. 1991;102 Pt 2:277-81.
969 28. Clement K, Rees H, Canver MC, Gehrke JM, Farouni R, Hsu JY, et al. CRISPResso2
970 provides accurate and rapid genome editing sequence analysis. Nat Biotechnol. 2019;37(3):224-
971 6.
972 29. Hwang G-H, Yu J, Yang S, Son WJ, Lim K, Kim HS, et al. CRISPR-sub: Analysis of
973 DNA substitution mutations caused by CRISPR-Cas9 in human cells. Computational and
974 Structural Biotechnology Journal. 2020;18:1686-94.
975 30. Shimonishi T, Sasaki M, Nakanuma Y. Precancerous lesions of intrahepatic
976 cholangiocarcinoma. J Hepatobiliary Pancreat Surg. 2000;7(6):542-50.
977 31. Kitadokoro K, Bordo D, Galli G, Petracca R, Falugi F, Abrignani S, et al. CD81
978 extracellular domain 3D structure: insight into the tetraspanin superfamily structural motifs.
979 EMBO J. 2001;20(1-2):12-8.
980 32. Goodman ZD. Grading and staging systems for inflammation and fibrosis in chronic liver
981 diseases. J Hepatol. 2007;47(4):598-607.
982 33. Bansal PS, Smout MJ, Wilson D, Cobos Caceres C, Dastpeyman M, Sotillo J, et al.
983 Development of a Potent Wound Healing Agent Based on the Liver Fluke Granulin Structural
984 Fold. J Med Chem. 2017;60(10):4258-66.
985 34. Jusakul A, Cutcutache I, Yong CH, Lim JQ, Huang MN, Padmanabhan N, et al. Whole-
986 Genome and Epigenomic Landscapes of Etiologically Distinct Subtypes of Cholangiocarcinoma.
987 Cancer Discov. 2017;7(10):1116-35.

988 35. Banales JM, Marin JJG, Lamarca A, Rodrigues PM, Khan SA, Roberts LR, et al.
989 Cholangiocarcinoma 2020: the next horizon in mechanisms and management. Nature Reviews
990 Gastroenterology & Hepatology. 2020;17(9):557-88.
991 36. Petney TN, Andrews RH, Saijuntha W, Wenz-Mucke A, Sithithaworn P. The zoonotic,
992 fish-borne liver flukes Clonorchis sinensis, Opisthorchis felineus and Opisthorchis viverrini. Int J
993 Parasitol. 2013;43(12-13):1031-46.
994 37. Mitacek EJ, Brunnemann KD, Suttajit M, Martin N, Limsila T, Ohshima H, et al.
995 Exposure to N-nitroso compounds in a population of high liver cancer regions in Thailand:
996 volatile nitrosamine (VNA) levels in Thai food. Food Chem Toxicol. 1999;37(4):297-305.
997 38. Sripa B, Tangkawattana S, Laha T, Kaewkes S, Mallory FF, Smith JF, et al. Toward
998 integrated opisthorchiasis control in northeast Thailand: the Lawa project. Acta Trop.
999 2015;141(Pt B):361-7.
1000 39. Gouveia MJ, Pakharukova MY, Laha T, Sripa B, Maksimova GA, Rinaldi G, et al.
1001 Infection with Opisthorchis felineus induces intraepithelial neoplasia of the biliary tract in a
1002 rodent model. Carcinogenesis. 2017;38(9):929-37.
1003 40. Kim E, Hart T. Improved analysis of CRISPR fitness screens and reduced off-target
1004 effects with the BAGEL2 gene essentiality classifier. Genome Med. 2021;13(1):2.
1005 41. Chai AWY, Yee PS, Price S, Yee SM, Lee HM, Tiong VK, et al. Genome-wide CRISPR
1006 screens of oral squamous cell carcinoma reveal fitness genes in the Hippo pathway. Elife.
1007 2020;9.
1008 42. Chaiyadet S, Krueajampa W, Hipkaeo W, Plosan Y, Piratae S, Sotillo J, et al.
1009 Suppression of mRNAs encoding CD63 family tetraspanins from the carcinogenic liver fluke
1010 Opisthorchis viverrini results in distinct tegument phenotypes. Sci Rep. 2017;7(1):14342.
1011 43. Tran MH, Pearson MS, Bethony JM, Smyth DJ, Jones MK, Duke M, et al. Tetraspanins
1012 on the surface of Schistosoma mansoni are protective antigens against schistosomiasis. Nat Med.
1013 2006;12(7):835-40.
1014 44. Wendt GR, Collins JN, Pei J, Pearson MS, Bennett HM, Loukas A, et al. Flatworm-
1015 specific transcriptional regulators promote the specification of tegumental progenitors in
1016 Schistosoma mansoni. Elife. 2018;7.
1017 45. Luo H, Lin Y, Liu T, Lai F-L, Zhang C-T, Gao F, et al. DEG 15, an update of the
1018 Database of Essential Genes that includes built-in analysis tools. Nucleic Acids Research.
1019 2020;49(D1):D677-D86.
1020 46. Pavani G, Amendola M. Targeted Gene Delivery: Where to Land. Front Genome Ed.
1021 2020;2:609650.
1022 47. Allen F, Crepaldi L, Alsinet C, Strong AJ, Kleshchevnikov V, De Angeli P, et al.
1023 Predicting the mutations generated by repair of Cas9-induced double-strand breaks. Nat
1024 Biotechnol. 2018.
1025 48. International Helminth Genomes C. Comparative genomics of the major parasitic worms.
1026 Nat Genet. 2019;51(1):163-74.
1027 49. Yang YM, Kim SY, Seki E. Inflammation and Liver Cancer: Molecular Mechanisms and
1028 Therapeutic Targets. Semin Liver Dis. 2019;39(1):26-42.
1029 50. Sripa B, Tangkawattana S, Sangnikul T. The Lawa model: A sustainable, integrated
1030 opisthorchiasis control program using the EcoHealth approach in the Lawa Lake region of
1031 Thailand. Parasitol Int. 2017;66(4):346-54.

1032 51. Fedorova OS, Fedotova MM, Zvonareva OI, Mazeina SV, Kovshirina YV, Sokolova TS,
1033 et al. Opisthorchis felineus infection, risks, and morbidity in rural Western Siberia, Russian
1034 Federation. PLoS Negl Trop Dis. 2020;14(6):e0008421.
1035 52. Chan-On W, Nairismagi ML, Ong CK, Lim WK, Dima S, Pairojkul C, et al. Exome
1036 sequencing identifies distinct mutational patterns in liver fluke-related and non-infection-related
1037 bile duct cancers. Nat Genet. 2013;45(12):1474-8.
1038 53. Ong CK, Subimerb C, Pairojkul C, Wongkham S, Cutcutache I, Yu W, et al. Exome
1039 sequencing of liver fluke-associated cholangiocarcinoma. Nat Genet. 2012;44(6):690-3.
1040 54. Chaisaingmongkol J, Budhu A, Dang H, Rabibhadana S, Pupacdi B, Kwon SM, et al.
1041 Common Molecular Subtypes Among Asian Hepatocellular Carcinoma and
1042 Cholangiocarcinoma. Cancer Cell. 2017;32(1):57-70 e3.
1043 55. Montal R, Sia D, Montironi C, Leow WQ, Esteban-Fabro R, Pinyol R, et al. Molecular
1044 classification and therapeutic targets in extrahepatic cholangiocarcinoma. J Hepatol.
1045 2020;73(2):315-27.
1046 56. Young ND, Gasser RB. Opisthorchis viverrini Draft Genome - Biomedical Implications
1047 and Future Avenues. Adv Parasitol. 2018;101:125-48.
1048 57. Frangoul H, Altshuler D, Cappellini MD, Chen YS, Domm J, Eustace BK, et al.
1049 CRISPR-Cas9 Gene Editing for Sickle Cell Disease and β-Thalassemia. N Engl J Med.
1050 2021;384(3):252-60.
1051 58. Fellmann C, Gowen BG, Lin PC, Doudna JA, Corn JE. Cornerstones of CRISPR-Cas in
1052 drug discovery and therapy. Nat Rev Drug Discov. 2017;16(2):89-100.
1053 59. Rizvi S, Khan SA, Hallemeier CL, Kelley RK, Gores GJ. Cholangiocarcinoma - evolving
1054 concepts and therapeutic strategies. Nat Rev Clin Oncol. 2018;15(2):95-111.
1055 60. Chansitthichok S, Chamnan P, Sarkhampee P, Lertsawatvicha N, Voravisutthikul P,
1056 Wattanarath P. Survival of Patients with Cholangiocarcinoma Receiving Surgical Treatment in
1057 an O. viverrini Endemic Area in Thailand: A Retrospective Cohort Study. Asian Pac J Cancer
1058 Prev. 2020;21(4):903-9.
1059 61. Chaiyarit P, Sithithaworn P, Thuwajit C, Yongvanit P. Detection of salivary antibodies to
1060 crude antigens of Opisthorchis viverrini in opisthorchiasis and cholangiocarcinoma patients. Clin
1061 Oral Investig. 2011;15(4):477-83.
1062 62. Mairiang E, Laha T, Kaewkes S, Loukas A, Bethony J, Brindley PJ, et al. Hepatobiliary
1063 morbidities detected by ultrasonography in Opisthorchis viverrini-infected patients before and
1064 after praziquantel treatment: a five-year follow up study. Acta Trop. 2021;217:105853.
1065 63. Sripa B, Suwannatrai AT, Sayasone S, Do DT, Khieu V, Yang Y. Current status of
1066 human liver fluke infections in the Greater Mekong Subregion. Acta Trop. 2021;224:106133.
1067 64. Charoensuk L, Ribas A, Chedtabud K, Prakobwong S. Infection rate of
1068 Opisthorchis viverrini metacercariae in cyprinoid fish from the markets and its association to
1069 human opisthorchiasis in the local community in the Northeast Thailand. Acta Trop.
1070 2022;225:106216.
1071 65. Pinlaor S, Onsurathum S, Boonmars T, Pinlaor P, Hongsrichan N, Chaidee A, et al.
1072 Distribution and abundance of Opisthorchis viverrini metacercariae in cyprinid fish in
1073 Northeastern Thailand. The Korean journal of parasitology. 2013;51(6):703-10.
1074 66. Piedrafita D, Spithill TW, Dalton JP, Brindley PJ, Sandeman MR, Wood PR, et al.
1075 Juvenile Fasciola hepatica are resistant to killing in vitro by free radicals compared with larvae
1076 of Schistosoma mansoni. Parasite Immunol. 2000;22(6):287-95.

1077 67. De Marco Verissimo C, Jewhurst HL, Dobó J, Gál P, Dalton JP, Cwiklinski K. Fasciola
1078 hepatica is refractory to complement killing by preventing attachment of mannose binding lectin
1079 (MBL) and inhibiting MBL-associated serine proteases (MASPs) with serpins. PLoS Pathog.
1080 2022;18(1):e1010226.
1081 68. Ran FA, Hsu PD, Wright J, Agarwala V, Scott DA, Zhang F. Genome engineering using
1082 the CRISPR-Cas9 system. Nature Protocols. 2013;8(11):2281-308.
1083 69. Montague TG, Cruz JM, Gagnon JA, Church GM, Valen E. CHOPCHOP: a
1084 CRISPR/Cas9 and TALEN web tool for genome editing. Nucleic Acids Research.
1085 2014;42(W1):W401-W7.
1086 70. Labun K, Montague TG, Gagnon JA, Thyme SB, Valen E. CHOPCHOP v2: a web tool
1087 for the next generation of CRISPR genome engineering. Nucleic Acids Research.
1088 2016;44(W1):W272-W6.
1089 71. Young ND, Nagarajan N, Lin SJ, Korhonen PK, Jex AR, Hall RS, et al. The Opisthorchis
1090 viverrini genome provides insights into life in the bile duct. Nat Commun. 2014;5:4378.
1091 72. Laha T, Pinlaor P, Mulvenna J, Sripa B, Sripa M, Smout MJ, et al. Gene discovery for the
1092 carcinogenic human liver fluke, Opisthorchis viverrini. BMC Genomics. 2007;8:189.
1093 73. Hulme BJ, Geyer KK, Forde-Thomas JE, Padalino G, Phillips DW, Ittiprasert W, et al.
1094 Schistosoma mansoni α-N-acetylgalactosaminidase (SmNAGAL) regulates coordinated parasite
1095 movement and egg production. PLoS Pathog. 2022;18(1):e1009828.
1096 74. Suyapoh W, Tangkawattana S, Suttiprapa S, Punyapornwithaya V, Tangkawattana P,
1097 Sripa B. Synergistic effects of cagA+ Helicobacter pylori co-infected with Opisthorchis viverrini
1098 on hepatobiliary pathology in hamsters. Acta Tropica. 2021;213:105740.
1099 75. Zen Y, Adsay NV, Bardadin K, Colombari R, Ferrell L, Haga H, et al. Biliary
1100 intraepithelial neoplasia: an international interobserver agreement study and proposal for
1101 diagnostic criteria. Modern pathology : an official journal of the United States and Canadian
1102 Academy of Pathology, Inc. 2007;20(6):701-9.
1103 76. Sato Y, Sasaki M, Harada K, Aishima S, Fukusato T, Ojima H, et al. Pathological
1104 diagnosis of flat epithelial lesions of the biliary tract with emphasis on biliary intraepithelial
1105 neoplasia. J Gastroenterol. 2014;49(1):64-72.
1106 77. Sudsarn P, Boonmars T, Ruangjirachuporn W, Namwat N, Loilome W, Sriraj P, et al.
1107 Combination of Praziquantel and Aspirin Minimizes Liver Pathology of Hamster Opisthorchis
1108 viverrini Infection Associated Cholangiocarcinoma. Pathology oncology research : POR.
1109 2016;22(1):57-65.
1110 78. Sudsarn P, Wongchalee N, Boonmars T, Laummaunwai P, Chamgramol Y, Pairojkul C,
1111 et al. Sex differences in opisthorchiosis and the development of cholangiocarcinoma in Syrian
1112 hamster model. Parasitol Res. 2014;113(3):829-35.
1113 79. Ishak K, Baptista A, Bianchi L, Callea F, De Groote J, Gudat F, et al. Histological
1114 grading and staging of chronic hepatitis. J Hepatol. 1995;22(6):696-9.
1115 80. Elkins DB, Haswell-Elkins M, Anderson RM. The epidemiology and control of intestinal
1116 helminths in the Pulicat Lake region of Southern India. I. Study design and pre- and post-
1117 treatment observations on Ascaris lumbricoides infection. Trans R Soc Trop Med Hyg.
1118 1986;80(5):774-92.
1119 81. Piratae S, Tesana S, Jones MK, Brindley PJ, Loukas A, Lovas E, et al. Molecular
1120 characterization of a tetraspanin from the human liver fluke, Opisthorchis viverrini. PLoS Negl
1121 Trop Dis. 2012;6(12):e1939.

82. Schmittgen TD, Livak KJ. Analyzing real-time PCR data by the comparative CT method. Nature Protocols. 2008;3(6):1101-8.
83. Theodorsson E. Resampling methods in Microsoft Excel for estimating reference intervals. Biochem Med (Zagreb). 2015;25(3):311-9.
84. Hwang GH, Yu J, Yang S, Son WJ, Lim K, Kim HS, et al. CRISPR-sub: Analysis of DNA substitution mutations caused by CRISPR-Cas9 in human cells. Comput Struct Biotechnol J. 2020;18:1686-94.
85. Park J, Lim K, Kim JS, Bae S. Cas-analyzer: an online tool for assessing genome editing results using NGS data. Bioinformatics. 2017;33(2):286-8.
86. Surget S, Khoury MP, Bourdon JC. Uncovering the role of p53 splice variants in human malignancy: a clinical perspective. Onco Targets Ther. 2013;7:57-68.
87. Nakayama M, Oshima M. Mutant p53 in colon cancer. Journal of Molecular Cell Biology. 2018;11(4):267-76.
88. Batheja N, Suriawinata A, Saxena R, Ionescu G, Schwartz M, Thung SN. Expression of p53 and PCNA in Cholangiocarcinoma and Primary Sclerosing Cholangitis. Modern Pathology. 2000;13(12):1265-8.
89. Rabacal W, Schweitzer F, Rayens E, Tarantelli R, Whang P, Jimenez VC, et al. Statin treatment prevents the development of pulmonary arterial hypertension in a nonhuman primate model of HIV-associated PAH. Scientific Reports. 2019;9(1):19832.
90. Hollenbach M, Thonig A, Pohl S, Ripoll C, Michel M, Zipprich A. Expression of glyoxalase-I is reduced in cirrhotic livers: A possible mechanism in the development of cirrhosis. PLoS One. 2017;12(2):e0171260.

1167 **Supporting information: Figures S1-S6 and Tables S1 and S2 (eight items).**
1168
1169
1170

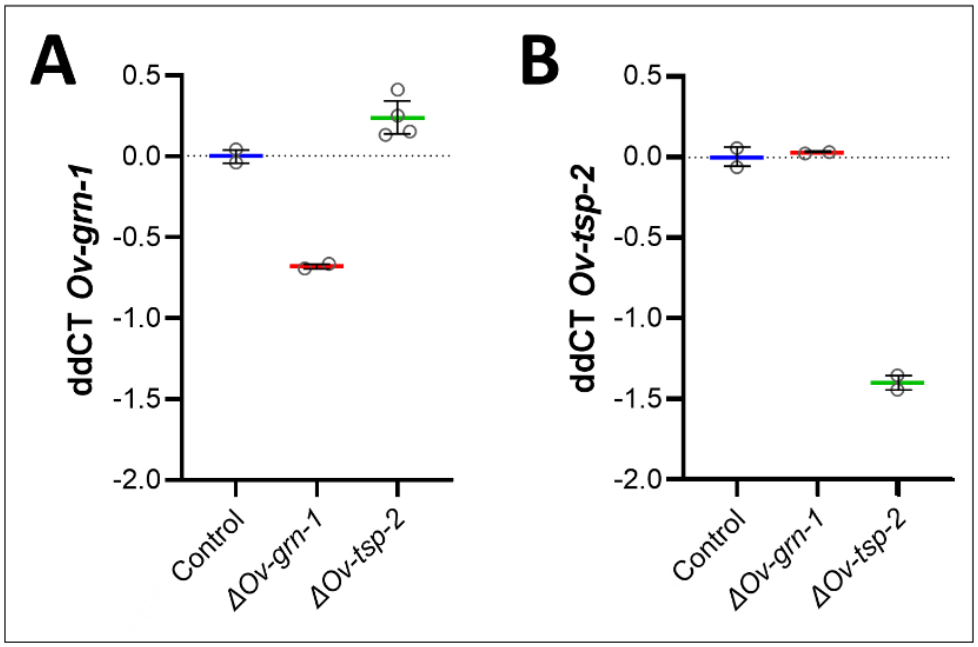

1171
1172
1173 ***Figure S1. Transcript levels of gene edited NEJ flukes with bootstrapped population values.***
1174 *Each group of flukes was subjected to gene editing targeting Ov-grn-1 (ΔOv-grn-1 flukes), Ov-*
1175 *tsp-2 (ΔOv-tsp-2 flukes), or an irrelevant guide RNA as a control (Control). Relative transcript*
1176 *levels were plotted for both Ov-grn-1* ***(A)*** *and Ov-tsp-2 genes* ***(B)*** *for all three groups: control*
1177 *flukes; ΔOv-grn-1 flukes, and ΔOv-tsp-2 flukes. Each panel shows ddCt (delta-delta cycle*
1178 *threshold) biological replicate values plotted relative to newly excysted juvenile (NEJ) control*
1179 *average. Resampling with replacement bootstrap analysis (B=1000) of ddCT scores used to*
1180 *generate population average denoted by thick colored line and 95% confidence interval error*
1181 *bars.*
1182
1183
1184
1185
1186

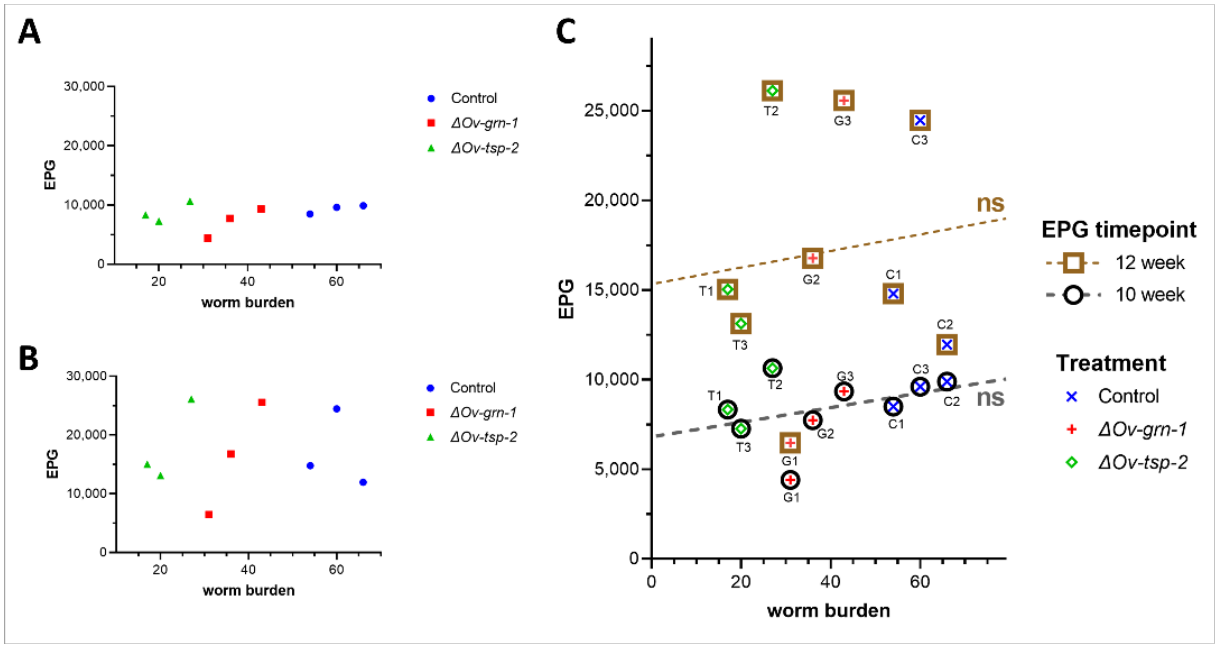

Figure S2. Experiment 1: Relationship of fecal egg count to worm burden. *Assessment of eggs per gram of feces (EPG) at 10* ***(A)*** *and 12* ***(B)*** *weeks after infection compared to worm burden at necropsy (week 14). The worm burden for each hamster was plotted against the EPG at weeks 10 and 12. Comparing these timepoints* ***(C)*** *with linear regression did not reveal variation from a line with zero slope (horizontal line) at both intervals. Each hamster was designated by letter, C= control, G=ΔOv-grn-1, T=ΔOv-tsp-2, with the number of the hamster, as 1, 2, and 3.*

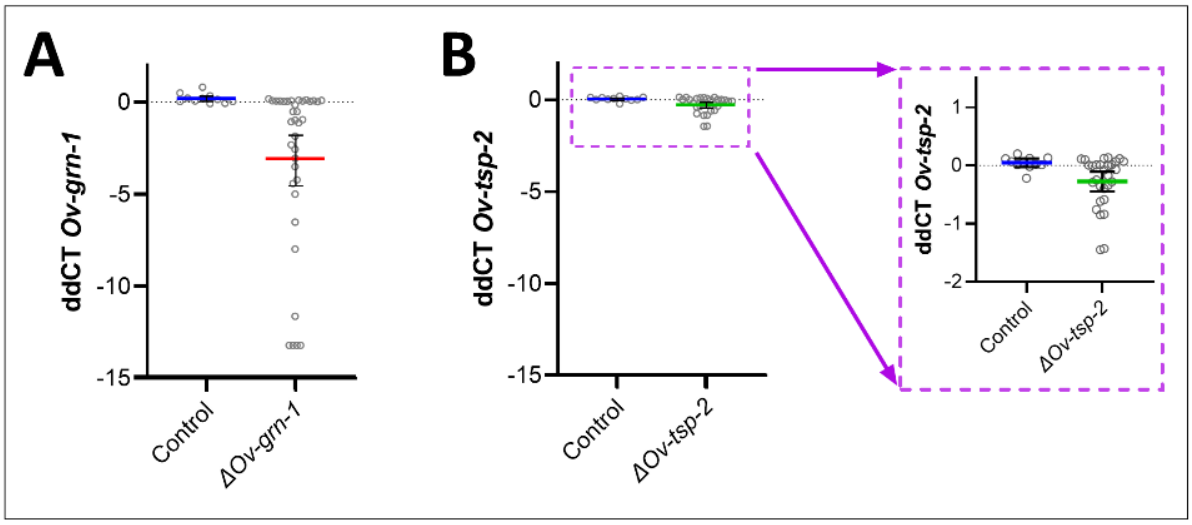

1216
1217
1218
1219 ***Figure S3. Experiment 1: Transcript levels of gene edited adult flukes with bootstrapped***
1220 ***population values***. *Each group of the flukes was subjected to gene editing targeting Ov-grn-1*
1221 *(ΔOv-grn-1 flukes), Ov-tsp-2 (ΔOv-tsp-2 flukes), or an irrelevant guide RNA as a control*
1222 *(Control). Each panel shows ddCt (delta-delta cycle threshold) of individual flukes plotted*
1223 *relative to transcript levels of wild-type flukes for Ov-grn-1 (**A**) and Ov-tsp-2 (**B**). The dashed*
1224 *line purple box inset is an enlarged section of panel B, included for clarity. Resampling with*
1225 *replacement bootstrap analysis (B=1000) of ddCT scores used to generate population average*
1226 *denoted by thick colored line and 95% confidence interval error bars.*
1227
1228
1229
1230
1231
1232
1233
1234

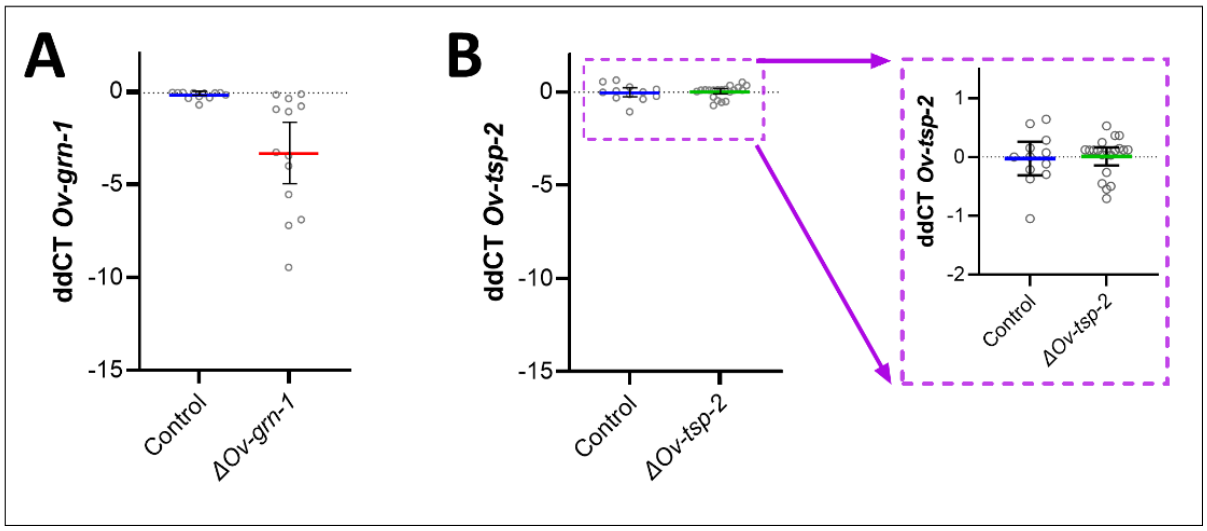

1235

1236 ***Figure S4. Transcript levels of adult flukes from Experiment 2 with bootstrapped population***
1237 ***values.*** *Each group of the 24 wk old flukes was subjected to gene editing targeting Ov-grn-1*
1238 *(ΔOv-grn-1 flukes), Ov-tsp-2 (ΔOv-tsp-2 flukes), or an irrelevant guide RNA as a control*
1239 *(Control). Each panel shows ddCt (delta-delta cycle threshold) for individual flukes plotted*
1240 *relative to wild-type (WT) fluke transcript levels for both Ov-grn-1 (A) and Ov-tsp-2 genes (B).*
1241 *The dashed line purple box inset is an enlarged section of panel B for clarity. Resampling with*
1242 *replacement bootstrap analysis (B=1000) of ddCT scores used to generate population average*
1243 *denoted by thick colored line and 95% confidence interval error bars.*
1244
1245
1246
1247
1248
1249
1250
1251
1252
1253
1254
1255
1256
1257
1258
1259
1260
1261
1262
1263
1264
1265
1266

.

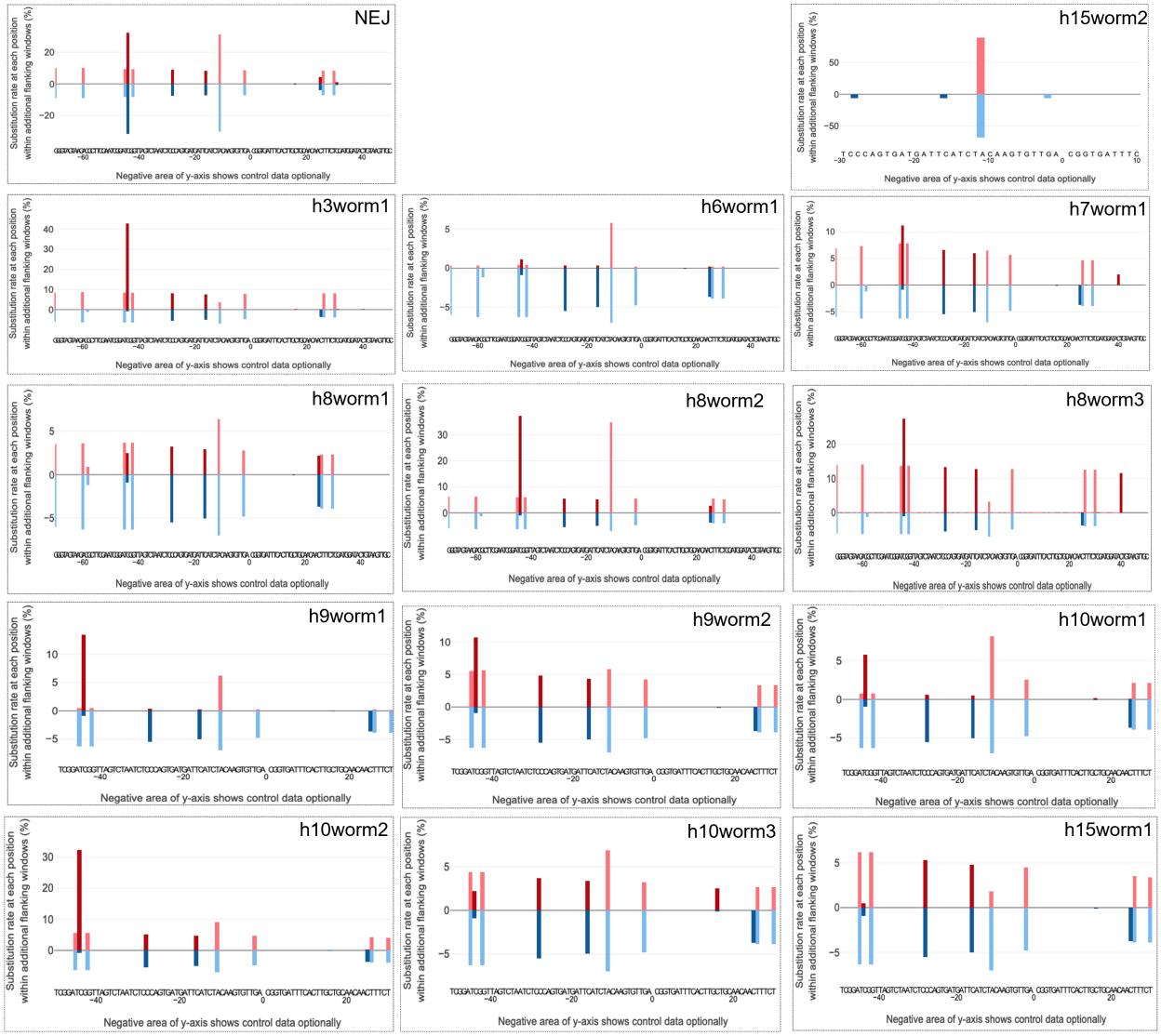

Figure S5. Profiles of nucleotide substitutions. *Nucleotide substitution profiles detected in the 173 bp amplicon spanning the programmed cleavage site of Ov-grn-1 from both juvenile (NEJ) and single adult O. viverrini flukes of the ΔOv-grn-1 treatment group compared with the irrelevant guide RNA treated control group. RGEN's CRISPR-sub analysis tool, http://www.rgenome.net/crispr-sub/#!, aligns read-pairs to plot the substitution patterns among Illumina sequence reads from amplicon libraries derived from CRISPR/Cas9 editing-focused datasets. Experimental group (red, upper axis) versus control group (blue, lower axis); the X-axis shows the targeted gene including programmed cleavage site (position 0) between nucleotides 19 and 20 of ORF 1 of Ov-grn-1. Juvenile flukes are shown in the top left and each adult fluke is shown separately and designated with the number of its host hamster number (x) 1-15 and worm number (y) 1-3: (h "x" worm "y"). Substantially differences in patterns of substitutions detected between the experimental and control groups were not apparent.*

1284
1285
1286
1287
1288
1289
1290

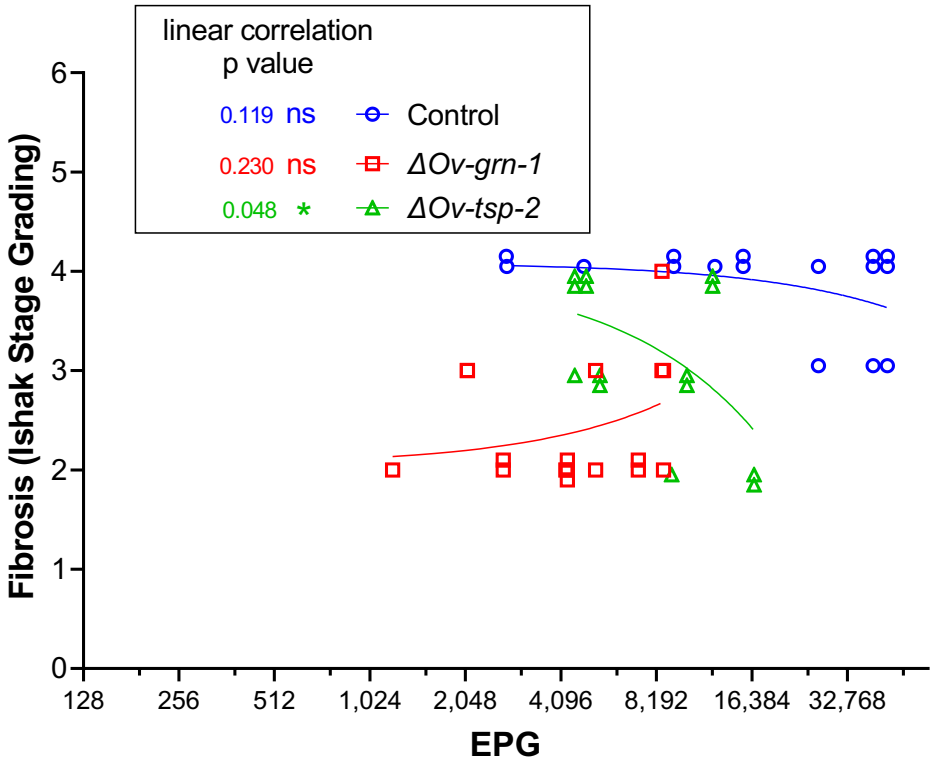

1291
1292
1293 ***Figure S6. Correlation between fecal EPG and fibrosis***. *For Experiment 2, each liver lobe was*
1294 *plotted as eggs per gram against the Ishak fibrosis (data combined from figure 3A and 6B).*
1295 *Data points have been nudged ± 0.1 on the vertical axis for clarity among overlapping points.*
1296 *The linear regression line for each group is shown; ns = not statistically significant; *, P ≤ 0.05.*
1297
1298

1299

Sample	Bases sequenced (Mbp)	Read depth	Read-pairs sequences	Read-pairs aligned (RPA)	RPA Unmodified reads	RPA Modified reads	RPA Insertions	RPA Deletions	Frameshift mutation (number,%)	Indel (%)
NEJs										
Control NEJs	26.3	152,023	113,442	51,402	51,384	18	0	18	0	**0.035%**
ΔOv-grn-1 NEJs	40.8	235,838	159,583	80,571	77,848	2,723	0	2,723	2 (0.02%)	**3.380%**
ADULT FLUKES										
Hamster 1-15: Control flukes	37.9	219,075	129,859	91,783	91,742	41	0	41	0	**0.045%**
$_{L}$ΔOv-grn-1 flukes (0-0.04% indels)										
Hamster 6: fluke 1	47.8	276,301	185,269	105,363	105,363	0	0	0	0	**0.000%**
Hamster 8: fluke 1	46.6	269,364	171,164	110,079	110,078	1	0	1	0	**0.001%**
Hamster 3: fluke 1	33.5	193,642	150,356	60,954	60,935	19	0	19	0	**0.031%**
Hamster 8: fluke 3	42.5	245,665	154,598	101,288	101,252	36	2	34	0	**0.036%**
Hamster 10: fluke 1	44.7	258,382	143,186	118,253	118,211	41	0	41	19 (48.8%)	**0.035%**
Hamster 9: fluke 1	62.7	362,428	193,741	168,806	168,741	65	0	65	0	**0.039%**
$_{M}$ΔOv-grn-1 flukes (3.1% indels)										
Hamster 8: fluke 2	48.1	278,035	169,500	116,021	112,458	3,563	1	3,563	8 (0.20%)	**3.071%**
$_{H}$ΔOv-grn-1 flukes (51-91% indels)										
Hamster 10: fluke 2	49.4	285,549	169,733	128,391	63,378	65,013	0	65,013	20 (0.03%)	**50.637%**
Hamster 15: fluke 2	53.1	306,936	166,531	143,206	64,899	78,307	1	78,307	0	**54.681%**
Hamster 7: fluke 1	46.7	269,942	182,260	102,168	27,617	74,551	0	74,551	0	**72.969%**
Hamster 10: fluke 3	47.5	274,566	161,903	120,064	26,447	93,617	0	93,617	22 (0.02%)	**77.973%**
Hamster 9: fluke 2	38.2	220,809	125,032	99,750	19,707	80,043	2	80,042	17 (0.02%)	**80.244%**
Hamster 15: fluke 1	45.3	261,850	155,792	115,881	10,413	105,468	1	105,468	0	**91.014%**

1300
1301
1302 ***Table S1. NGS sequencing data summary.*** *Frequency of successful CRISPR/Cas9 gene knock*
1303 *out editing as determined by frameshift mutations. The CRISPResso2 analysis used a window*
1304 *size (-3 option) that include the whole 173 bp amplicon, except 25 bp at each end in order to the*
1305 *exclude the primer regions. Combined insertions and deletions are used to generate the Indel%,*
1306 *the proportion of read-pairs aligned (RPA). To match the color scheme in the figures the control*
1307 *groups highlighted in blue and low, medium and highly edited adults are highlighted in red,*
1308 *purple and green. Note that the vast majority of indels are located in the 5' UTR and are not*
1309 *frameshift mutations.*
1310
1311
1312
1313
1314

Parameters Groups	Control	*ΔOv-grn-1*	*ΔOv-tsp-2*
CCA development			
CCA positive hamsters/total hamsters (% positive)	10/12 (83.33%)	9/13 (69.23%)	7/13 (53.85%)
Histopathological diagnosis			
Dysplasia (precancerous lesion)	2	1	2
Low grade CCA	2	5	1
High grade CCA	8	4	6
CCA histopathological type			
Tubular	9	8	4
Papillary/Cystic	0	1	0
Mucinous	1	0	3
CCA location (lobe)			
Right	6	5	4
Left	1	2	2
Middle	0	0	1
Right and Left	2	1	0
Right and Middle	1	0	0
Right, Middle and Left	0	1	0
Tumor progression			
Focal	6	5	1
Fully developed	4	4	6

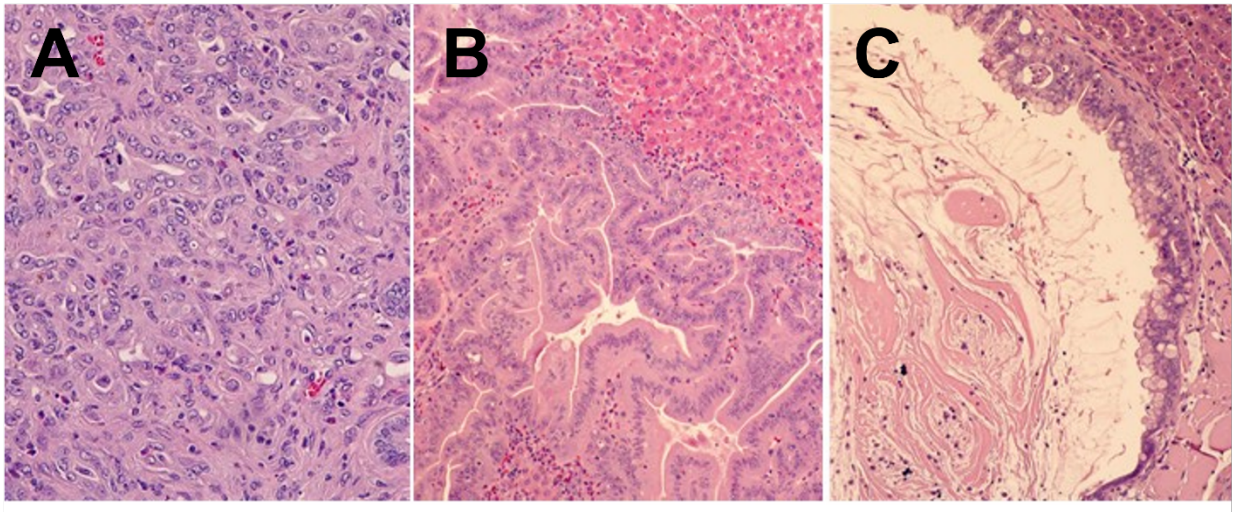

Table S2. Pathology assessment on development of pre-malignant and malignant lesions. *The table shows the pathogenesis outcomes from the 3 groups of hamsters and the histopathological diagnosis data was summarized as graphs in Figure 5. Beyond Figure 5, the table describes the CCA histopathological type, location, and tumor progression. Below the table histological images show the three major histopathological types:* ***A*** *= tubular;* ***B*** *= papillary; and* ***C*** *= mucinous CCA.*